A detailed mineralogical, petrographic, and geochemical study of the highly reduced chondrite, Acfer 370

Journal Item

A detailed mineralogical, petrographic and geochemical study of the highly reduced chondrite, Acfer 370

Giovanni Pratesi[1,2], Stefano Caporali[3], Richard C. Greenwood[4], Vanni Moggi Cecchi[5], Ian A. Franchi[4]

[1] Dipartimento di Scienze della Terra, Università degli Studi di Firenze,
Via Giorgio La Pira, 4 – 50121 Firenze (Italy)
[2] INAF-IAPS, Via Fosso del Cavaliere 100 – 00133 Roma (Italy)
[3] Dipartimento di Ingegneria Industriale, Università degli Studi di Firenze,
Via Santa Marta, 3 – 50139 Firenze (Italy)
[4] Planetary and Space Sciences, The Open University, Milton Keynes, MK7 6AA UK
[5] Museo di Storia Naturale, Università degli Studi di Firenze,
Via Giorgio La Pira, 4 – 50121 Firenze (Italy)

Corresponding author's e-mail address
giovanni.pratesi@unifi.it

ABSTRACT

Among the many ungrouped meteorites, Acfer 370, NWA 7135 and El Médano 301 – probably along with the chondritic inclusion in Cumberland Falls and ALHA 78113 – represent a homogeneous grouplet of strongly reduced forsterite-rich chondrites characterized by common textural, chemical, mineralogical and isotopic features. All of these meteorites are much more reduced than OCs, with a low iron content in olivine and low-Ca pyroxene.

In particular, Acfer 370 is a type 4 chondrite that has olivine and low-Ca pyroxene compositional ranges of Fa 5.2-5.8 and Fs 9.4-33.4, respectively. The dominant phase is low-Ca pyroxene (36.3 vol%), followed by Fe-Ni metal (16.3 vol%) and olivine (15.5 vol%); nevertheless, considering the Fe-oxyhydroxide (due to terrestrial weathering), the original metal content was around 29.6 vol%. Finally, the mean oxygen isotopic composition $\Delta^{17}O$ = +0.68‰ along with the occurrence of a silica phase, troilite, Ni-rich phosphides, chromite and oldhamite confirm that these ungrouped meteorites have been affected by strong reduction and are different from any other group recognized so far.

INTRODUCTION

Chondrites account for more than 90 percent of all the known meteorites. Among them, ordinary chondrites (OC) are by far the most abundant class (over 51,000 records in the Meteoritical Bulletin Database) followed, to a much lesser extent, by carbonaceous chondrites (CC) and enstatite chondrites (EC). Two further much less populated classes are the Kakangari (K) chondrites (four known meteorites) and Rumuruti (R) chondrites (201 official records on the Meteoritical Bulletin Database at the time of writing).

It is well known that OCs show a wide range in oxidation state, from the H group (more reduced) to the LL group (more oxidized). An even more reduced group (or grouplet), called HH chondrites or low-FeO ordinary chondrites (McCoy et al. 1994; Russell et al. 1998; Toriano et al. 2011) may exist, although currently such chondrites are classified as H-anomalous (see Meteoritical Bulletin Database).

Some meteorites do not fit into these more populated and well-defined groups of chondrites and are designated "ungrouped". Acfer 370 is one such chondrite. Here we present the results of a detailed investigation of the petrography, geochemistry, and isotopic composition of Acfer 370. Based on the results of these studies we examine the relationship between Acfer 370 and other related chondrite groups.

In 2002, the meteorite collector Filiberto Ercolani was prospecting in the Acfer area (Sahara Desert, Algeria) and found a small meteorite (129g), which lacked fusion crust. This meteorite was acquired in 2009 by the Museum of Planetary Science of the Prato Province (Tuscany, Italy) and was characterized and classified by Moggi Cecchi et al. (2009) and subsequently given the official name Acfer 370.

Acfer 370 has been recognized as having similar characteristics ($Fa_{5.6\pm0.2}$; low-Ca pyroxene $Fs_{15.7\pm6.9}$) to chondritic inclusions found in the Cumberland Falls and ALHA 78113 aubritic breccias (Moggi Cecchi et al. 2009). However, in contrast to these inclusions, Acfer 370 is a homogeneous, discrete specimen and not a fragment or clast embedded in another meteorite.

Over the following years two other unique ungrouped chondrites (NWA 7135 and El Médano 301), which share characteristics with the Cumberland Falls and ALHA 78113 chondritic clasts, have been found and studied. NWA 7135 was purchased from a Moroccan dealer at the 2010 Munich Mineral Show. It is a type 3 chondrite of relatively high petrologic subtype (>3.7), with most olivines $<Fa_{4.8}$ and only a few grains $>Fa_{6.2}$ (Irving et al., 2015). El Médano 301 was found in 2013 during a scientific expedition searching for meteorites in the Atacama Desert (Chile). It is a chondrite containing olivine and low-Ca pyroxene with a mean composition of $Fa_{3.9\pm0.3}$ and $Fs_{12.8\pm4.9}$, respectively (Pourkhorsandi et al., 2016; Pourkhorsandi et al., 2017).

The nature of the relationship between the more populated chondritic groups and the clasts found in Cumberland Falls and ALHA 78113 has been the subject of significant debate. In particular, Rubin (2010) inferred an OC, rather than an enstatite chondrite or carbonaceous chondrite, parentage for these inclusions. This designation was based on their bulk chemical composition, O-isotopic composition, chondrule size distribution, the occurrence of barred olivine (BO) and radial pyroxene (RP) chondrules, chondrule modal abundance data and the core composition of low-Ca pyroxenes. Rubin (2010) concluded that the Cumberland Falls chondritic clasts are probably derived from an OC projectile that collided with the aubrite parent body and suffered a reduction process as a consequence of compositional re-equilibration with the aubritic host. In contrast, Kuehner et al. (2016), while recognizing that the Cumberland Falls chondrite clasts differ from their Northwest African counterparts in being more equilibrated and also more shocked, hypothesized that they originated from the collision of a forsterite-rich chondritic impactor into the aubrite parent body. In this study, we present a detailed petrographic, geochemical and oxygen isotopic study of Acfer 370. This study highlights the similarities between Acfer 370, NWA 7135 and El Médano 301 and also the chondritic inclusions in Cumberland Falls and ALHA 78113. These samples all represent highly reduced material, related to, but fully distinguishable from, the more populated ordinary chondrites groups.

EXPERIMENTAL

Samples

Three thin sections of Acfer 370 (Acfer 370,1; 370,2; 370,3), each about 6 cm^2 area, were prepared starting from the main mass belonging to the collection of the Museum of Planetary Science of the Prato Province (Museo di Scienze Planetarie, Prato, inv. MSPO 2277). In order to get these sections, the hand-size sample was split into two end cuts weighing 67 and 62 grams.

Techniques and methods

Optical microscopy analyses were performed at the Department of Earth Sciences of the University of Florence (Dipartimento di Scienze della Terra, Università degli Studi di Firenze) by means of a Zeiss Axioplan II optical microscope equipped with a Zeiss Axiocam camera.

Electron Dispersive X-ray Spectrometry (EDS) microanalysis and elemental mapping were undertaken both at the Department of Chemistry of the University of Firenze using a Hitachi SEM equipped with a NORAN System-6 software and at the MEMA laboratories of the University of Firenze using a Zeiss EVO MA15 equipped with a 10 mm^2 Silicon Drift Detector (SDD) and OXFORD INCA 250 microanalysis software. In order to get the relative modal abundances of mineral phases, single element X-ray maps of Na, K, Al, Mg, Fe, and Ca (resolution 5x5 μm) were obtained. Using an INCA software module, the layers were combined, and the histogram function was used to determine the percentage of each mineral present in the specimen. Finally, the PAP correction method (Pouchou & Pichoir, 1987) has been applied to the acquired data.

Quantitative mineral analyses of the main phases (olivine and pyroxene) were performed, at the microanalysis laboratory of the IGG-CNR using a JEOL JXA-8600 Electron Microprobe equipped with four wavelength dispersive spectrometers (WDS). Operating conditions were 15 keV accelerating voltage, 20 nA beam current, a beam size of 1 μm and data acquisition in wavelength-dispersive spectrometry (WDS) mode. The following Astimex standards have been used for the analyses: olivine, diopside, sanidine, albite, chromite, bustamite, apatite. Anorthite (USNM 137041), augite (USNM 122142) and ilmenite (USNM 96189), provided by Smithsonian Institution, were also used as standards.

Oxygen isotopic analysis was undertaken at the Open University using an infrared laser fluorination system (Miller et al. 1999; Greenwood et al. 2017). Laser fluorination analyses were undertaken on a powdered sample produced by crushing and homogenizing a clean interior chip of Acfer 370 with a mass of 150 mg. This chip was selected from the less-weathered portion of the meteorite. Prior to fluorination 15.9 mg of this homogenized powder was washed in ethanolamine thioglycollate (EATG) (Greenwood et al. 2012). EATG treatment has proved to be efficient at selectively removing Fe-rich weathering products, such as those that form by oxidation of Fe,Ni metal and can result in significant shifts in the oxygen isotope composition of metal and sulphide-rich meteorites (Greenwood et al. 2012). After washing in EATG 12.0 mg of powder remained, representing a 24.5 % loss in weight. From this EATG-treated powder ~2 mg aliquots were loaded into a Ni sample block and this was placed into a two-part chamber, made vacuum-tight using a compression seal with a copper gasket and a quick-release KFX clamp (Miller et al. 1999).

A 3 mm-thick BaF_2 window at the top of the chamber allowed simultaneous viewing and laser heating of the samples. After sample loading, the cell was heated under vacuum for a minimum of 24 hours and to a temperature of at least 70°C to remove any adsorbed atmospheric moisture. Prior to fluorination, the system blank was systematically reduced by flushing the chamber with aliquots of BrF_5, such that the final blank was less than 60 nmol O_2. Sample heating in the presence of BrF_5 was carried out using an integrated 50 W infrared CO_2 laser (10.6 μm) and video system mounted on an X-Y-Z gantry supplied by Photon Machines Inc. (Greenwood et al. 2017). After fluorination, the released O_2 was purified by passing it through two cryogenic (liquid nitrogen) traps and over a bed of heated KBr. The isotopic composition of the purified oxygen was analyzed using a Thermo Fisher MAT 253 dual-inlet mass spectrometer (mass resolving power, 200). Interference at m/z = 33 by NF^+ was monitored by performing scans for NF_2^+ on the sample gas before analyzing each sample; this was below interference levels during all sample analyses reported here. Our current system precision based on repeat analyses (n = 39) of our obsidian internal standard is ±0.052‰ for $\delta^{17}O$, ±0.094‰ for $\delta^{18}O$, and ±0.017‰ for $\Delta^{17}O$ (2σ) (Starkey et al. 2016). Both for the analyses of Acfer 370 and other related samples (NWA 7135, El Medano 301, Cumberland Falls inclusions), $\Delta^{17}O$ has been calculated as: $\Delta^{17}O = \delta^{17}O - 0.52\ \delta^{18}O$ in order to be able to directly compare these more recent data with the ordinary chondrite analyses of Clayton et al. (1991).

Trace element concentrations were measured at the Open University using an Agilent 7500a ICP-MS. The analytical procedures followed were essentially the same as those detailed by Barrett et al. (2017) and Hunt et al. (2017).

RESULTS

Petrography

Acfer 370 is a rounded, slightly flattened and partially oriented stone, lacking fusion crust. Overall, the meteorite is characterized by a distinct chondritic texture (Fig. 1) showing – in thin section – mostly circular and closely packed chondrules, chondrule fragments and olivine crystals, both euhedral and fragmental. Sometimes, elongated chondrules, opaque nodules and metal veins tend to form an assemblage that seems to be aligned along a preferred orrientation. All the known types of chondrules (PO=porphyritic olivine, POP=porphyritic olivine-pyroxene, PP=porphyritic pyroxene, GP-GOP=granular pyroxene, granular olivine-pyroxene, RP=radial pyroxene, BO=barred olivine, C=cryptocrystalline), representing about 70% volume of the meteorite, occur in the specimen (Fig. 3). The chondrules are embedded within opaque material's matrix (mainly composed of iron metal and its weathering products, but also comprising sulphides, phosphides, enstatite laths and olivine crystals) accounting for ~ 30% volume. The metal is pervasive and has surrounded and sometimes invaded the chondrules (along the fractures). As pointed out by Pourkhorsandi et al. (2017) in the case of El Médano 301, the texture of this "matrix" often appears similar to the remnant of metal/sulphides-silicate intergrowths observed in some enstatite chondrites (Lin and Kimura, 1998; van Niekerk and Keil, 2006; Rubin and Wasson, 2011; Horstmann et al. 2014). This texture is also observed in some areas of Acfer 370, where such intergrowth occurs as fine enstatite laths in altered metal (Fig. 9e).

Chondrules type and size

Chondrules were deemed intact if they exhibited ≥ 270° of arc or if their texture is clearly visible, otherwise they have been classified as chondrule fragments or relict chondrules, respectively. Chondrules account for ~70% of the meteorite's total volume: ~50% are intact chondrules, the remaining are chondrule fragments and loose olivine crystals. Some chondrules contain interstitial devitrified glass with microlites. Many chondrules contain metal blebs. We distinguished textural types, inside the porphyritic type, according to the olivine/pyroxene modal ratio (Gooding and Keil, 1981). PO chondrules are defined as those with a ratio ≥ 10:1 and PP those possessing a ratio ≤ 1:10; the chondrules with ratios intermediate are defined as POP.

Accurate measurements, carried out by optical microscopy on 500 chondrules, provides the following size parameters: diameter range 130-2300 μm, arithmetic mean 593 μm, geometric mean 523 μm, median 530 μm, standard deviation 310 μm. As suggested by Friedrich et al. (2015), we also calculated the lognormal distribution which takes into account the asymmetric probability density function of chondrule size frequency (Fig. 4) obtaining a mean value of 523 μm.

A study of abundance and size distributions for each chondrule type was also performed, in order to compare these data with similar ones collected on other meteorite groups. The results of this investigation are shown in Fig. 5. The GP-GOP type chondrules are the most common, accounting for 22% of the total, whereas BO type chondrules are the least common, accounting for only 5% of the total. Porphyritic chondrules (PO-POP-PP) amount to 50% vol of the total, whereas nonporphyritic chondrules (as defined by Nehru et al. 1994) amount to 23% of the total.

Although Gooding and Keil (1981) excluded any dependence of chondrule size and shape on textural types, we investigated the size-frequency distribution vs textural types (Fig. 5 and Table 1). The mean chondrule sizes, in order of decreasing mean apparent diameter, are as follows: PO

(655 µm), RP (620 µm), POP (565 µm), PP (510 µm), GP-GOP (465 µm), C (410 µm), BO (400 µm). The application of Kolmogorov-Smirnov non-parametric test (Till, 1974), commonly used to compare two population distributions of unknown form, confirm that inside the entire set of porphyritic chondrules PO > POP (confidence level 96%), PO > PP (confidence level 99%), POP > PP (confidence level 80%), whereas inside the set of nonporphyritic chondrule RP > GP-GOP > C > BO (confidence level 99%).

Mineralogy and Mineral Chemistry

Analyses by optical microscopy, electron microscopy images, as well as X-ray maps obtained by means of SEM-EDS, provided information about modal mineralogy. As displayed in Table 2 and in Figure 6, the main phases in Acfer 370 are low-Ca pyroxene, Fe-Ni metal, Mg-rich olivine, high-Ca pyroxene, devitrified feldspar normative glass mesostasis containing plagioclase microlites, troilite; minor phases are represented by chromite, hydroxylapatite, schreibersite and oldhamite (Fig. 9).

Olivine

Olivine occurs both inside (Figs. 3, 8) and outside the chondrules and accounts for about 15 vol% of the specimen. The size of olivine crystals inside the chondrules depends on the chondrule diameter and type; crystals outside the chondrules are euhedral or fragmental and range from 350 to 1800 µm but some polycrystalline aggregates may exceed 2000 µm. Although the crystals are often heavily fractured, they are not mosaicized and do not show planar fractures or undulose extinction, indicative of significant shock-induced deformation.

An interesting characteristic of all the olivine crystals is their magnesium-rich composition. EPMA analyses, performed on olivine inside and outside chondrules, provided a $Fa_{5.5}$ content (mean on 16 analyses, PMD = 3.0%), confirms that olivine is compositionally homogeneous. Finally, an assessment of minor elements shows a moderate MnO content (0.4-0.5 wt%), a very low Cr_2O_3 content (≤0.07 wt%) while Al_2O_3, TiO_2, CaO, CoO, NiO, V_2O_5 fall below the detection limit (see Table 3).

Pyroxene

Pyroxenes are mainly found inside chondrules (POP, PP, GP-GOP, RP) or chondrule fragments; only rarely do they occur outside the chondrules, or near the margin of metal grains, as low-Ca pyroxene laths. Both low- and high-Ca pyroxenes are present in Acfer 370 (Table 2), accounting for about 36 vol% and 6 vol% of the specimen, respectively. Low-Ca pyroxenes occur both as clino- and orthoenstatite, sometimes showing polysynthetic twinning.

Depending on the different type of chondrules, pyroxenes exhibit a wide variety of textures and their compositions define a relatively large compositional field (Table 4 and Fig. 7), even within a single chondrule. A comparison with the compositional distribution fields of UOC, OC and EC clearly indicates that the pyroxenes in Acfer 370 are unequilibrated and similar to those found in UOC.

According to the nomenclature for pyroxenes suggested by Rock (1990), their compositions (Table 4) range from enstatite to ferroan enstatite, from magnesium-rich pigeonite to calcian magnesium-rich pigeonite, from subcalcic magnesium-rich augite to magnesium-rich augite, even though diopside and ferroan diopside may occasionally occur (Fig. 7). Usually, the low-Ca pyroxene crystals and grains show normal zoning, with the inner portion richer in magnesium (enstatite) and the outer portion richer in iron (ferroan enstatite) (Figs. 8b, 8f, 8j). Sometimes enstatite grains are rimmed by Mg-rich pigeonite (Fig. 8f) or Mg-rich augite (Fig. 8c).

In addition to the occurences mentioned above, pigeonite, augite and diopside are also present as elongated laths in the Na-Al rich mesostasis (Fig. 8d) and as large euhedral crystals (Fig. 8h), or as skeletal crystals (Fig. 8l, 8n, 8p). Although uncommon, zoned high-Ca pyroxenes have been observed. In one example, within a POP chondrule, crystals of calcian Mg-rich pigeonite ($Wo_{11}En_{71}Fs_{18}$) rimmed by Mg-rich Augite ($Wo_{30}En_{55}Fs_{15}$) were observed. Aluminium content in

pyroxenes is variable but, in both low- and high-Ca pyroxenes, it tends to increase along with Ca content. Indeed, the more Ca-rich augite (CaO > 19 wt%) can reach up to 11 wt% of Al_2O_3 (Table 4).

Plagioclase and plagioclase-glass

In Acfer 370, mesostasis was detected as an interstitial phase among olivine, low- and high-Ca pyroxene crystals. Usually mesostasis is turbid and contains skeletal low- or high-Ca pyroxene crystals (Figs. 8l, 8n, 8p); sometimes it constitutes the preferred carrier of small metal blebs (Figs. 8b, 8n). Nevertheless, portions of clear glass mesostasis can also be found, mainly in PO chondrules.

Quantitative compositional data were difficult to obtain due to the small size of the areas; however, this phase is usually Na-rich, although the Na content is variable among different chondrules (Fig. 8). Cryptocrystalline chondrules (Fig. 8g) have devitrified glass with $Ab_{66,}$ whereas other chondrules contain glass or devitrified glass characterized by Ab_{92} (Figs. 8f). However, within a single chondrule, the composition is homogeneous.

Iron-nickel metal

Unaltered Fe-Ni metal is the most abundant opaque phase in the meteorite accounting for nearly 16 vol%, although in a large part of the specimen, it has been completely converted into Fe-oxyhydroxide. Outside the chondrules, iron and its alteration products are ubiquitous and may occur as distinct large grains (up to 500 μm in size), large or narrow veins, blebs and droplets (Fig. 9). Inside chondrules more variable features occur, with some chondrules containing a large amount of metal, whereas in others it is almost absent (Fig. 9). The distribution of metal within individual chondrules is often highly variable. Frequently, where metal is present inside chondrules, it is often hosted by mesostasis glass, but may also be contained in pyroxenes. In the latter case, it prevails in the ferroan enstatite rather than in enstatite or high-Ca pyroxenes. It is noteworthy that forsterite, inside or outside the chondrules, is almost completely free of iron metal.

Metal (Table 5) contains 6.06-6.34 wt% Ni and 0.30-0.43 wt% Co whereas the Si-content is ≤ 0.05 wt% (that is the detection limit in our analysis). In contrast to what has been observed in El Médano 301 (Pourkhorsandi et al. 2017), taenite has not been detected in Acfer 370, although its presence cannot be ruled out.

Accessory phases

Both opaque and transparent accessory phases have been detected in Acfer 370 (see Tables 2 and 5for their compositions). Troilite is the main accessory phase in the specimen (~ 1.6 vol%) and generally contains no other elements apart from small amounts of Cr (0.30 wt%) and rare Ni (from < 0.12 to 0.34). Other accessory opaque phases consist of oxides, sulphides and phosphides, whose representative compositions are displayed in Table 5. Members of the spinel group are dominated by the presence of chromite, occurring as euhedral or subhedral grains (with sizes ranging from a few microns to tens of microns) mainly inside silicates (both pyroxenes and olivine), between silicates grains or near to metal. Phosphides are mainly represented by nickelphosphide; when schreibersite occurs, it always shows Ni contents higher than 40 wt%. It is important to note the presence of the rare mineral phase oldhamite (Fig. 9), which occurs as rounded or angular grains, up to ~ 200 μm, within the metallic matrix.

Among the transparent phases, we can report the occurrence of apatite supergroup minerals occurring as grains with a maximum dimension of tens of microns. They are generally located at or near the boundaries of iron metal grains. EDS spectra do not display any trace of chlorine or fluorine and, therefore, the species is reasonably assigned to hydroxylapatite.

Classification

Petrologic type

Sharp, well defined chondrule outlines and the hetereogeneity of pyroxene compositions would suggest a petrologic type 3 (subtype >3.7 as suggested by Irving et al 2015 for NWA 7135), although the homogeneity of olivine points towards petrologic type 4.

According to the recommendations established for H-L-LL ordinary chondrites (Grossman 2011), values of 3.0% PMD-FeO in olivine and 28.4% PMD-FeO in pyroxene (corresponding respectively to 0.96 σ-Fa and 5.6% σ-Fs), indicate a petrologic type 4 for Acfer 370. Even though petrologic type ≥ 3.7 is still compatible with the calculated PMD-FeO values for pyroxene, it is not compatible with the low PMD-FeO (i.e. with the composition homogeneity) of olivine. On the basis of these considerations and in contrast to the original description (Weisberg et al., 2008), we suggest type 4 for Acfer 370.

Weathering grade and shock stage

The specimen shows two areas characterized by different weathering grades (Fig. 2). One area, corresponding to the lighter portion, is only slightly affected by oxidation, so that metal and sulfides are clearly visible in both optical and electron microscopy. In contrast, the other area, corresponding to the darker portion, is affected by heavy alteration with all the metal being replaced by Fe-oxyhydroxides (only sulphide grains remained). Therefore, according to the proposed weathering scale (Wlotzka, 1993; Wlotzka et al., 1995; Al-Kathiri et al. 2005; Zurfluh et al. 2016), a grade ranging from W2 to W4 can be inferred.

Stelzner et al. (1999), who studied weathered meteorites from the Acfer region, suggested that in thin section weathering effects usually decrease from the outside to the interior of the meteorite. However, evolved gas analysis indicates that variation in weathering between surface and core is not significant with respect to the formation of Fe-oxyhydroxides (Stelzner et al. 1999). Our observations would agree with this latter inference, as weathering in Acfer 370, as well as the formation of Fe-oxyhydroxides, has not proceeded uniformly from exterior to interior and is asymmetrically distributed in the specimen.

Olivine grains show a few irregular fractures; nevertheless, the sharp optical extinction observed in all grains, without any trace of undulatory extinction indicates a shock stage of S1 according to the scheme of Stöffler et al. (1991).

Chemistry

Trace-element bulk chemistry

Acfer 370 (Table 6) displays a high siderophile element content, confirming that metal plays an important role in the mineralogical composition of this meteorite. An additional noteworthy feature is the high Ba content, which probably reflects the influence of terrestrial weathering (Pourkhorsandi et al., 2017). Acfer 370 also has a high content of Pb and U.

Oxygen isotopic composition

The results of oxygen isotope analysis are given in Table 7. The mean value for Acfer 370 plots within the field of H group chondrites in Fig. 10

DISCUSSION

Relationship to other reduced ordinary chondrites

The meteorites discussed in this paper are mineralogically and compositionally distinct from previously described reduced ordinary chondrite groups (e.g. Wasson et al., 1993; Russell et al., 1998). Thus, Acfer 370, NWA 7135, El Médano 301 and the inclusions in CF and ALHA 78113 are significantly more reduced than the low-FeO and HH chondrites described in these earlier studies

(Wasson et al., 1993; Russell et al., 1998). Acfer 370 and related samples are characterized by a much lower olivine Fa composition e.g. ~5 mol%; whereas the low-FeO and HH chondrites are ~15 mol% (Wasson et al., 1993; Russell et al., 1998). In addition, Acfer 370 and related samples are characterised by a higher Ni-content in phosphides, as well as by the occurrence of very reduced phases such as oldhamite. These differences clearly indicate a distinct provenence for the earlier described reduced ordinary chondrites, which may simply represent a somewhat more reduced extension of the main H chondrite group. In contrast, Acfer 370 and related samples are compositionally distinct materials which are most likely derived from a distinct parent body to that of the extended H chondrite association.

Comparison with NWA 7135, El Médano 301, CF and ALHA 78113.

Petrography and mineralogy

As discussed above, Acfer 370, as well as NWA 7135 and El Médano 301, represent discrete specimens, whereas chondritic inclusions in Cumberland Falls (CF) and ALHA 78113 are black or white clasts (whose areas vary from tens to hundreds mm^2) often angular, sometimes coherent and, at times, intimately intermixed with the aubrite host (Lipschutz et al., 1988). This is an important difference, because it answers the question posed by Lipschutz et al. (1988): "whether Cumberland Falls inclusions are related to discrete meteorites is uncertain", but also provides an opportunity to investigate a larger and therefore more statistically significant sample of this meteorite type.

As concerns the classification of chondrules and their relative abundance, no information has been provided yet for clasts in CF and ALHA 78113, whereas NWA 7135 and El Médano 301 have been well characterized (Irving et al. 2015; Pourkhorsandi et al. 2017). Porphyritic chondrules (POP, PO, PP) are dominant both in Acfer 370 and in El Médano, whereas the relative abundance of the other chondrule types may be slightly different: RP, GP-GOP, C, BO in El Médano; GP-GOP, RP, C, BO in Acfer 370. There appears to be little difference in the average apparent chondrule diameter among these three meteorites: in fact, the average apparent chondrule diameter is around 523 μm for Acfer 370 (geometric mean), 502 μm for El Médano 301 and 476 μm for NWA 7135. A possible reason for these slight differences may be due to much better counting statistics for Acfer 370 (n=500) in comparison with those provided by Pourkhorsandi et al. (2017) for El Médano 301 (n=99) and NWA 7135 (n=132).

The modal content of olivine and pyroxene, both high-Ca and low-Ca, in Acfer 370 (Table 2) is lower than the range observed for CF clasts, although it is compatible with the range in ALHA 78113. On the other hand, there are some differences between Acfer 370 and El Médano 301 (e.g. olivine 15.5 vs. 8 vol%; low-Ca pyroxene 36.3 vs. 42 vol%).

It is important to point out that Fe-Ni metal content appears to separate the reduced chondrites (Acfer 370, El Médano 301 and possibly NWA 7135) from the reduced inclusions (CF and ALHA 78113). Thus, in Acfer 370 the Fe-Ni metal content is high (the total amount of weathering products + unaltered Fe-Ni metal, sulphides and phosphides is around 30 vol%) with similar amounts in El Médano 301 (no data are provided in literature for NWA 7135). In contrast, the amount of Fe-Ni metal in the inclusions of CF and ALH A78113 is much lower (at a maximum of 8.5 and 5.3 vol% respectively). The reason for this difference is unclear. It may be related to some form of post emplacement reprocessing in the case of the inclusions. Alternatively, the reduced chondrites and inclusions may, despite their compositional similarities, represent genetically unrelated material. These possibilities require further investigation.

Another major phase in Acfer 370, El Médano 301 and NWA 7135, as well in CF and ALH A78113 clasts, is microlites-rich devitrified plagioclase-glass, whereas chromite is an accessory phase observed in Acfer 370, El Médano 301 and NWA 7135 alone. Hydroxylapatite and chlorapatite also occur as accessory phases, respectively in Acfer 370 and in El Médano 301.

Schreibersite and nickelphosphide have been detected in all the above-mentioned meteorites, except El Médano 301. A noteworthy occurrence, in terms of accessory minerals, concerns the calcium sulfide oldhamite found in CF clasts, Acfer 370 and NWA 7135; in El Médano 301 only calcium sulphate grains, that may represent weathered oldhamite, have been found.

Mineral chemistry

Generally, the composition of silicate and opaque phases is quite similar in CF, ALHA 78113, Acfer 370, NWA 7135 and El Médano 301, although some differences are present.

Olivine

As displayed in Table 8, the compositional range of olivine in Acfer 370 ($Fa_{5.2-5.8}$), CF clasts (Fa_{1-5}), NWA 7135 ($Fa_{4.8-6.2}$) and El Médano 301 ($Fa_{3.5-5.0}$) are similar, although they are much narrower compared to the olivine composition of ALHA 78113 (Fo_{2-21}). Moreover, olivine in Acfer 370, ALHA 78113 and El Médano 301 contains more MnO (0.40-0.50 wt%) compared to CF clasts (0.11-0.14 wt%), whereas the contents of Cr_2O_3 and CaO are similar in CF clasts (Rubin, 2010) and in Acfer 370, NWA 7135 and El Médano 301. In all these meteorites, Ca, Al, Ti, Co and Ni are always below detection limits. It is noteworthy that Rubin (2010) observed olivine grains containing numerous small grains of low-Ni metallic Fe in the chondritic clasts of CF, whereas in Acfer 370 (apart from a few exceptions) the olivine crystals are usually lacking in metallic Fe.

Pyroxenes

In contrast to olivine, which is compositionally homogeneous, low-Ca pyroxenes have undergone only partial equilibration during metamorphism. Therefore, pyroxenes in Acfer 370, as well as in the other ungrouped meteorites studied here, are compositionally variable and show common characteristics in all these meteorites (Table 8). Any variability present does not seem to be related to particular petrographic features: no systematic relationships occur among the different type of chondrules and, moreover, there are no differences in the pyroxene composition between the interior and exterior portions of chondrules. Nevertheless, according to Lipschutz et al. (1988), in CF clasts some variability may be linked to different types of matrix: pyroxenes in small black matrix clasts were found to be generally more Fe-rich than those in large chondritic clasts. However, those small clasts were similar to the large CF clasts in being consistently more Fe-rich than the co-existing olivine, another indication that all the clasts form part of the same population.

Due to lack of complete equilibration, the composition of low-Ca pyroxene spans a realtively large range in Fs content, varying from a minimum of $Fs_{0.3}$ (in CF) to a maximum of $Fs_{33.4}$ (in Acfer 370). Despite their overall similarity, the mean Fs content is variable between each of the reduced chondrites discussed here, with El Médano 301 (11.4 mol%) having a lower value than CF (14.2 mol%), NWA 7135 (14.8 mol%), Acfer 370 (16.7 mol%) and ALH A78113 (23 mol%). Acfer 370 and NWA 7135 contain both pigeonite and calcic pigeonite; moreover they display normal zoning in low-Ca pyroxenes (more Fe-rich rims), showing no trace of the reverse zoning sometimes observed in El Mèdano 301.

High-Ca pyroxenes display a very large compositional range, among the ungrouped chondrites discussed here. In particular, Acfer 370 contains sub-calcic augite as has also been seen in NWA 7135, but it also contains augite as is present in CF and ALHA 78113. Neal and Lipschutz (1981) found in CF a solid solution that they interpreted as jadeitic pyroxene and considered this to be the result of a late massive collisional event. Such a jadeitic component has not been found in NWA 7135, El Médano 301 and Acfer 370.

Plagioclase and plagioclase-glass

In the ungrouped chondrites considered in this study, plagioclase is present in the clasts and chondrules only as a fine-grained or glassy component. As a result of forming a fine-scale intergrowth with mafic minerals, some FeO and MgO is detected in all analyses of the glass.

According to Lipschutz et al. (1988), feldspathic glass in ALHA 78113,41 is unusual in comparison with the composition of the feldspar in Acfer 370, CF inclusions as well as the other fragments of ALHA 78113; in fact, it has very low CaO (0.1-0.4 wt%), and high Na_2O (11-14 wt%) contents. On the other hand, feldspathic glass in ALHA 78113,49 is generally albitic, but some areas have the composition of nepheline: SiO_2 (45 wt%); Al_2O_3 (32wt%); Na_2O (16 wt%); K_2O (5 wt%).

FeNi metal

Iron (kamacite) is the dominant metallic phase in these ungrouped chondrites and its composition ranges from 3.4 (in ALHA 78113) to 6.7% Ni (in El Médano 301). Although there are extensive replacements by weathering products in some of them, the overall Ni content is very similar among these meteorites. No correlations between Ni and other features have been observed either in Acfer 370, NWA 7135 and El Médano 301, although Neal and Lipschutz (1981) observed that mean Ni contents in CF chondritic inclusions generally decreased and Si increased (up to 0.22 wt%) as ordered by Fs content. Other elements may occur in the metal, although in very low amount (Tables 5 and 8): Cr < 0.07 wt.%, P is around 0.10 wt%, Si content is ≤0.25 wt%, whereas Co ranges from 0.30 to 0.53 wt%.

A search for taenite in Acfer 370 was unsuccessful, as was also the case in a study performed by Binns (1969) on one inclusion in CF. Conversely, Neal and Lipschutz (1981) and Pourkhorsandi et al. (2017) were able to find taenite intergrowths with iron (kamacite) sufficiently large to permit analysis respectively in CF and El Médano 301.

Troilite

No systematic trends arise from the mean troilite analyses reported in the literature. Nevertheless, according to Lipschutz et al. (1988), troilite grains in the chondritic clasts of ALHA 78113 compositionally differ somewhat from one another (e.g. one clast contains troilite with 0.3% Ni, 0.06% Cr and <0.02% Ti; in another clast troilite has 0.2% Ni, 0.7% Cr and 0.6% Ti). In Acfer 370 troilite always contains small amounts of Cr (mean 0.30 wt%), just like troilite in CF (mean 0.28 wt%), and very low amounts of Ni; troilite of CF also has a low Mn content (mean 0.17 wt%) (Neal and Lipschutz, 1981). Data for troilite in NWA 7135 and El Médano 301 is not currentlt available. Information about the occurrence of troilite in NWA 7135 appears to be ambiguous, since Irving et al. (2015) observed Cr-free pyrrhotite, whereas Kuehner et al. (2015) detected troilite.

Schreibersite and nickelphosphide

Fe-Ni phosphides are distinctive markers in all the specimens considered in this study, with the exception of El Médano 301, where their absence is probably due to the high weathering grade. The composition of schreibersite is peculiar (Table 7), being unusually rich in Ni in Acfer 370, and sometimes in CF. In these meteorites the molar Ni/(Fe+Ni) ratio sometimes exceeds 50% and consequently becomes nickelphosphide. Lower Ni contents, 18% and 19.6 wt%, were measured in ALHA 78113 and CF respectively. Neal and Lipschutz (1981) emphasized that, in one section of CF, some schreibersite grains seemed free of contact with metal and those few had distinctly higher Fe/Ni ratios than grains in contact with metal. Moreover, mean Fs content of low-Ca pyroxene and the Fe (hence, Ni) content of schreibersite appeared roughly correlated: the lower the mean Fs content of pyroxene in an inclusion the higher the Fe/Ni ratio in the schreibersite. Two grains of schreibersite in NWA 7135, analyzed during this study, showed values of Ni ranging from 35.6 wt% to 36.8 wt%.

Phosphates

Acfer 370, as well as El Médano 301 (Pourkhorsandi et al. 2017), contain subhedral or anhedral grains of apatite (respectively hydroxyapatite and chlorapatite), whereas this phase has not been detected in the other meteorites discussed in this study. On the other hand, merrillite and

brianite-like phosphate were found by Lipschutz et al. (1988) in two ALHA 78113 chondritic clasts. The brianitic phosphate was fine-grained and therefore difficult to analyze.

Other phases

Chromite spinels have been found in Acfer 370, NWA 7135 and El Médano 301 (Kuehner et al., 2015; Pourkhorsandi et al. 2017). Where the meteorite has experienced significant weathering (e.g. El Médano 301), spinel may be the sole phase to survive in the terrestrial environment (Pourkhorsandi et al. 2017). Another interesting phase, found in both Acfer 370 and NWA 7135, is a silica phase within pyroxene-rich chondrules, as also observed by Pourkhorsandi et al. (2017) in El Médano 301.

Chemistry

Trace-element bulk chemistry

The trace-element composition of Acfer 370 can only be compared to that of El Médano 301, as no data have been provided by Irving et al. (2015) and Kuehner et al. (2015). Data in Table 6 shows enrichments of V (×1.5), Cu (×2), Sr (×2), Ba (×4), Pb (×10) and U (×2) in Acfer 370 compared to El Médano 301; on the other hand, El Médano 301 – in comparison with Acfer 370 – shows enrichments of Ga (×2.5), Rb (×1.5), Mo (×2.8), Cs (×6.8), La (×2), Ce (×1.7), Pr (×1.5) and Th (×2.2). These differences in the bulk elemental composition could be related not only to a different weathering grade, but also differing weathering processes that occurred in different environments (Stelzner et al., 1999; Barrat et al., 2001). Moreover, it should be remembered that the amount of material used for these analyses is always very low and as a result a slight difference in modal mineralogy can determine differences in the bulk chemistry.

Oxygen isotopes

Acfer 370 (EATG treated) has a lower $\delta^{18}O$ value than NWA 7135 (Irving et al., 2015; Kuehner et al., 2015), chondritic inclusions in Cumberland Falls (Kuehner et al., 2016) and El Médano 301 (Pourkhorsandi et al., 2017) (Fig. 10). In the case of NWA 7135 and El Médano 301 this may reflect the presence of residual terrestrial weathering products. As noted previously, El Médano 301, in particular, has experienced significant levels of terrestrial alteration and despite acid leaching, the influence of this process on its oxygen isotopic composition may not have been entirely removed. As pointed out by Stelzner et al. (1999) in their study of three H5 chondrites showing different weathering grades, the effect of weathering is to increase the $\delta^{18}O$ value and decrease the $\Delta^{17}O$ value of a meteorite. Cumberland Falls is a fall and hence its higher $\delta^{18}O$ value in comparison to Acfer 370 is primary and may reflect modal differences between the two samples, such as a higher content of feldspar in Cumberland Falls compared to Acfer 370.

In Figure 10 Acfer 370 plots within the H chondrite field. This relationship suggests that there may be a genetic link between the H chondrites and Acfer 370. The chondritic inclusion in Cumberland Falls and NWA 7135 have slightly lower $\Delta^{17}O$ values than Acfer 370. However, this does not preclude a genetic relationship between these three samples as in the case of Cumberland Falls the presence of any aubritic host material would lower the bulk $\Delta^{17}O$ value and any residual weathering products in NWA 7135 would have the same effect. The higher $\Delta^{17}O$ value of El Médano 301 is more problematic. If its $\delta^{18}O$ value has been increased by the presence of residual weathering products this should also lower its $\Delta^{17}O$ further. The relatively high $\Delta^{17}O$ value of El Médano 301 would appear to preclude the possibility of a simple mass-dependent fractionation relationship with Acfer 370 or any of the other reduced chondrites discussed here. On the other hand, the $\Delta^{17}O$ composition of El Médano 301 is within the range shown by the H group chondrites. This again may indicate a genetic relationship between the H chondrites and these ungrouped reduced chondrites. Alternatively, the variation in $\Delta^{17}O$ seen in these ungrouped chondrites is a reflection of their primary oxygen isotope heterogeneity.

CONCLUSIONS

Acfer 370 is a type 4 strongly reduced chondrite, displaying distinctive textural, mineralogical, petrological and chemical features. Texturally, it is characterized by abundant chondrules embedded in an opaque matrix, mainly composed of FeNi metal and its weathering products. Silicate phases are mainly represented by low-Ca pyroxene, olivine, plagioclase and devitrified plagioclase-glass and, to a lesser extent, by high-Ca pyroxene.

All these features are shared with two other anomalous chondrites, NWA 7135 and El Médano 301, which would appear to have formed in a similar setting to Acfer 370. All three of these meteorites show some features in common with those of the chondritic inclusions found in Cumberland Falls and ALH A78113. Nevertheless, these chondritic inclusions probably experienced some degree of reduction subsequent to emplacement within their host lithologies and hence their initial mineral chemistries are somewhat uncertain.

Evidence in favor of very reducing conditions during the formation of Acfer 370, NWA 7135 and El Médano 301 is strong. This evidence includes: the very low Fe content of olivine; the high amount of free metal; the very low amount of Si and Cr in the Fe-Ni metal (kamacite); the peculiar composition of schreibersite (being very rich in Ni up to become nickelphosphide, as well as the low amount of Si in these phosphides); the low amount of Cr in troilite; the occurrence of a silica phase and oldhamite. The oxygen isotopic composition of these meteorites suggests that there may be a genetic link with the H ordinary chondrite group. This can best be explained by both having formed from similar nebular precursors, but with the ungrouped reduced chondrites having experienced more reducing conditions, either before accretion or subsequently on their parent body. Based on the evidence presented here, it seems most likely that the reduced chondrites represent a distinct group, albeit with affinities to the H group ordinary chondrites.

Acknowledgments

The authors are indebted to the Italian Ministry of Education, University and Research as well as to the University of Firenze for financial support of the project respectively through the funds FFABR 2017 “Fondo per il finanziamento delle attività base di ricerca” and University of Firenze Annual Research Funds 2018. We thank Sam Hammond for her help with ICP-MS trace element analysis at the Open University. Oxygen isotope studies at the Open University are funded by a consolidated grant from the Science and Technology Facilities Council (STFC), UK. We thank Adrian J. Brearley for editorial handling and very useful suggestions, and Alan Rubin, Michael K. Weisberg and Bertrand Devouard for their constructive reviews.

REFERENCES

Al-Kathiri A., Hofmann B.A., Jull A.J.T., and Gnos E. 2005. Weathering of meteorites from Oman: Correlation of chemical and mineralogical weathering proxies with ^{14}C terrestrial ages and the influence of soil chemistry. *Meteoritics & Planetary Science* 40:1215-1239.

Barrat J. A., Blichert-Toft J., Nesbitt R. W., and Keller F. 2001. Bulk chemistry of Saharan shergottite Dar al Gani 476. *Meteoritics & Planetary Science* 36:23-29.

Barrett T. J., Mittlefehldt D. W., Greenwood R. C., Charlier B. L. A., Hammond S. J., Ross D. K., Anand M., Franchi I. A., Abernethy F. A. J., and Grady M. M. 2017. The mineralogy, petrology, and composition of anomalous eucrite Emmaville. *Meteoritics & Planetary Science* 52:656-668.Binns

R.A. 1969. A chondritic inclusion of unique type in the Cumberland Falls meteorite, pp. 696-704, in Meteorite Research, P. M. Millman, ed. (D. Reidel, Dordrecht, Holland).

Clayton R.N. and Mayeda T.K. 1978. Genetic relations between iron and stony meteorites. *Earth Planet. Sci. Lett.* 40:168-174.

Clayton R.N., Mayeda T.K., Goswami J.N., and Olsen E.J. 1991. Oxygen isotope studies of ordinary chondrites. *Geochimica et Cosmochimica Acta* 55:2317-2337.

Friedrich J.M., Weisberg M.K., Ebel D.S., Biltz A.E., Corbett B.M., Iotzov I.V., Khan W.S., and Wolman M.D. 2015. Chondrule size and related physical properties: A compilation and evaluation of current data across all meteorite groups. *Chemie der Erde* 75:419-443.

Gooding J.L. and Keil K. 1981. Relative abundances of chondrule primary textural types in ordinary chondrites and their bearing on condition of chondrule formation. *Meteoritics* 16:17-43.

Grady M.M., Pratesi G., and Moggi Cecchi V. 2014. Atlas of Meteorites. Cambridge University Press, 384 p.

Greenwood R.C., Franchi I.A., Gibson J. M., and Benedix G.K. 2012. Oxygen isotope variation in primitive achondrites: The influence of primordial, asteroidal and terrestrial processes. *Geochimica et Cosmochimica Acta* 94:146-163.

Greenwood R.C., Burbine T.H., Miller M.F, and Franchi I.A. 2017. Melting and differentiation of early-formed asteroids: The perspective from high precision oxygen isotope studies. *Chemie der Erde* 27:1-43.

Grossmann J.N. 2011. White paper report for the Nomenclature Committee on the composition of olivine and pyroxene in equilibrated ordinary chondrites.
https://www.lpi.usra.edu/meteor/docs/whitepaper-supp.pdf

Hunt A. C., Benedix G. K., Hammond S. J., Bland P. A., Rehkamper M., Kreissig K., Strekopytov S., 2017. A geochemical study of the winonaites: Evidence for limited partial melting and constraints on the precursor composition. *Geochimica et Cosmochimica Acta* 199:13-30.

Horstmann M., Humayun M., and Bishoff A. 2014. Clues to the origin of metal in Almahata Sitta EL and EH chondrites and implications for primitive E chondrite thermal histories. *Geochimica et Cosmochimica Acta* 140:720-744.

Irving A.J., Kuehner S.M., Ziegler K., Kuntz F., and Sipiera P.P. 2015. Northwest Africa 7135: an unusual reduced, unequilibrated chondrite containing oldhamite, daubréelite, schreibersite and djerfisherite, and with a unique oxygen isotopic composition. *46th Lunar and Planetary Science Conference*, abs. 2437.

Kuehner S.M., Irving A.J., Ziegler K., Sanborn M.E., and Yin Q. 2015. F3/4 Chondrite Northwest Africa 7135: further assessment of its relationship to clasts in the Cumberland Falls aubrite. *78th Annual Meeting of the Meteoritical Society*, abs. 5238.

Kuehner S.M., Wittke J.H., Ziegler K., and Irving A.J. 2016. Mineralogy and oxygen isotopic composition of exotic F6 chondrite clasts in the Cumberland Falls aubrite. *47th Lunar and Planetary Science Conference*, abs. 2304.

Lin Y. and Kimura M. 1998. Petrographic and mineralogical study of new EH melt rocks and a new enstatite chondrite grouplet. *Meteoritics & Planetary Science* 33:501-511.

Lipschutz M.E., Verkouteren R.M., Sears D.W.G., Hasan F.A., Prinz M., Weisberg M.K., Nehru C.E., Delaney J.S., Grossman L., and Boily M. 1988. Cumberland Falls chondritic inclusions: III. Consortium study of relationship to inclusions in Allan Hills 78113 aubrite. *Geochimica et Cosmochimica Acta* 52:1835-1848.

McCoy T. J., Keil K., Scott E. R. D., Benedix G. K., Ehlmann A.J., Mayeda T. K. and Clayton, R. N. (1994) Low-FeO ordinary chondrites: a nebular origin and new chondrite parent body. *Lunar and Planetary Science Conference XXV*. Lunar Planet. Inst., Houston, TX. pp. 865–866 (abstr.).

Miller M.F., Franchi I.A., Sexton A.S., and Pillinger C.T. 1999. High precision $\delta^{17}O$ isotope measurements of oxygen from silicates and other oxides: Method and applications. *Rapid Communications in Mass Spectrometry* 13:1211–1217.

Moggi Cecchi V., Pratesi G., Franchi I.A., and Greenwood R.C. 2009. Acfer 370: an anomalous chondrite related to the Cumberland Falls breccia. *72nd Annual Meteoritical Society Meeting*, abs. 5421.

Morimoto N., Fabries J., Ferguson A.K., Ginzburg I.V., Ross M., Seifert F.A., Zussman J., Aoki K., and Gottardi G. 1988. Nomenclature of pyroxenes. *American Mineralogist* 73:1123-1133.

Neal C. W. and Lipschutz M. E. 1981. Cumberland Falls chondritic inclusions: Mineralogy/petrology of a forsterite chondrite suite. *Geochimica et Cosmochimica Acta* 45:2091-2095, 2097-2107.

Nehru C.E., Weisberg M.K., and Prinz M. 1994. Porphyritic versus nonporphyritic chondrules. In *Lunar and Planetary Inst., Papers Presented to the Conference on Chondrules and the Protoplanetary Disk* p 26-27.

Pouchou J.L. and Pichoir F. 1987. Basic expression of "PAP" computation for quantitative EPMA, in Proc. 11th ICXOM (eds. J.D. Brown and R.H. Packwood), University of Western Ontario, London, Ontario, pp. 249-253.

Pourkhorsandi H., Gattacceca J., Devouard B., D'Orazio M., Rochette P., Beck P., Valenzuela M., and Sonzogni C. 2016. El Médano 301: a new forsterite chondrite. *79th Annual Meeting of the Meteoritical Society*, abs. 6176.

Pourkhorsandi H., Gattacceca J., Devouard B., D'Orazio M., Rochette P., Beck P., Sonzogni C., and Valenzuela M. 2017. The ungrouped chondrite El Médano 301 and its comparison with other reduced ordinary chondrites. *Geochimica et Cosmochimica Acta* 218:98-113.

Rock N.M.S. 1990. The International Mineralogical Association (IMA/CNMMN) pyroxene nomenclature scheme: computerization and its consequences. *Mineralogy and Petrology* 43:99-119.

Rubin A.E. 2010. Impact melting in the Cumberland Falls and Mayo Belwa aubrites. *Meteoritics & Planetary Science* 45:265-275.

Rubin A.E. and Wasson J.T. 2011. Shock effects in "EH6" enstatite chondrites and implications for collisional heating of the EH and EL parent asteroids. *Geochimica et Cosmochimica Acta* 75:3757-3780.

Russell S.S., McCoy T.J., Jarosewich E. and Ash R.D. 1998. The Burnwell, Kentucky, low iron oxide chondrite fall: Description, classification and origin. *Meteoritics & Planetary Science* 33:853-856.

Starkey N.A., Jackson C.R.M., Greenwood R.C., Parman S., Franchi I.A., Jackson M., Fitton J.G., Stuart F.M., Kurz M., and Larsen L.M. 2016. Triple oxygen isotopic composition of high-^{3}He/^{4}He mantle. *Geochimica et Cosmochimica Acta* 176:227-238.

Stelzner Th., Heide K., Bischoff A., Weber D., Scherer P., Schultz L., Happel M., Schrön W., Neupert U., Michels R., Clayton R.N., Mayeda T.K., Bonani G., Haidas I., Ivy-Cohs S., and Suter M. 1999. An interdisciplinary study of weathering effects in ordinary chondrites from the Acfer region, Algeria. *Meteoritics & Planetary Science* 34:787-794.

Stöffler D., Keil K., and Scott E.R.D. 1991. Shock metamorphism of ordinary chondrites. *Geochimica et Cosmochimica Acta* 55:3845-3867.

Till R. 1974. Statistical Methods for the Earth Scientist: An Introduction. Wiley, New York, New York, USA. 154 pp.

Toriano J., Rumble D., Rivers M.L. and Friedrich J.M. 2011. Composition of three low-FeO ordinary chondrites: Indications of a common origin with the H chondrites. *Geochimica et Cosmochimica Acta* 75:6511-6519.

Van Niekerk D. and Keil K. 2006. Classification of five news ordinary chondrites from North West Africa. *Chemie der Erde* 66:153-158.

Verkouteren R.M. and Lipschutz M.E. 1983. Cumberland Falls chondritic inclusions. II: Trace element contents of forsterite chondrites and meteorites of similar redox state. *Geochimica et Cosmochimica Acta* 47:1625-1633.

Wasson J. T., Rubin A. E. and Kallemeyn G. W. (1993) Reduction during metamorphism of four ordinary chondrites. *Geochimica et Cosmochimica Acta* 57:1867-1889.

Weisberg M.K., Smith C., Benedix G., Folco L., Righter K., Zipfel J., Yamaguchi A. and Chennaoui Aoudjehane H. 2008. The Meteoritical Bulletin, No. 94, September 2008. *Meteoritics & Planetary Science* 43:1551–1588.

Wlotzka F. 1993. A weathering scale for the ordinary chondrites (abstract). *Meteoritics* 28, 460.

Wlotzka F., Jull A. J. T. and Donahue D. J. 1995. ^{14}C terrestrial ages of meteorites from Acfer, Algeria. In *Workshop on Meteorites from Cold and Hot Deserts* (eds. L. Schultz, J.O. Annexstad and M.E. Zolensky), pp. 72-73. LPI Tech. Rpt. 95-02, Lunar and Planetary Institute, Houston, Texas, USA.

Zurfluh F.J., Hofmann B.A., Gnos E., Eggenberger U., and Jull A.J.T. 2016. Weathering of ordinary chondrites from Oman: Correlation of weathering parameters with ^{14}C terrestrial ages and a refined weathering scale. *Meteoritics & Planetary Science* 51:1685-1700.

Table 1 – Main features of the several textural types of chondrules observed in Acfer 370

Chondrule Type	N total of chondrules	Mean size	Standard deviation	Standard error	Geometric mean	Geometric SD	Minimum	Median	Maximum
PO	84	720	320	30	655	2	200	640	1800
POP	91	620	290	30	565	2	200	560	1800
PP	76	570	270	30	510	2	190	515	1280
GP-GOP	110	510	240	20	465	2	140	455	1560
BO	25	460	250	50	400	2	130	370	1110
RP	57	710	410	50	620	2	180	640	2300
C	57	490	330	40	410	2	140	370	1800

Table 2 – Comparison of modal composition (vol%) for Acfer 370, El Médano 301 and NWA 7135. Data from CF and ALHA 78113 inclusions have also been reported.

	Acfer 370	[1]El Médano 301	[2]NWA 7135	[3]Cumberland Falls inclusions	[3]ALHA 78113 Inclusions
Olivine	15.5	8	d	19.1-33.8	10.3-50.5
Low-Ca pyroxene	36.3	42	d	39.7-52.5	17.4-55.8
High-Ca pyroxene	6.1	6	d	6.6-25.5	4.0-21.6
Plagioclase and plagioclase-glass	10.8	9	d	0-10.6	5.1-15.9
Silica phase	d	d	nd	nd	nd
Oldhamite	d	d (?)	d	d	nd
Roedderite	nd	nd		nd	0.0-3.7
Chromite	0.9	d	d	nd	0.0-0.2
Hydroxylapatite	0.8	Chlorapatite		0.0-0.1	d
Fe-Ni metal	16.3*	d	d	0.0-8.5	2.2-5.3
Troilite	1.6*	d	d	1.0-2.4	2.0-2.8
Schreibersite/Ni-phosphide	0.5*	nd	d	0.0-0.2	trace-5.9
Cr-free pyrrothite	nd	nd	d	nd	nd
Djerfisherite	nd	nd	d	nd	0.0-0.8
Daubréelite	nd	nd	d	0.0-0.3	trace-0.3
Alabandite	nd	nd	nd	0.0-0.2	nd
Weathering products	11.2				
Weathering products + unaltered Fe-Ni metal, sulphides and phosphides.	29.6	32			

Data from: [1] Pourkhorsandi et al. (2017); [2] Kuehner et al. (2015) and Irving et al. (2015); [3] Lipschutz et al. (1988).
d = detected, although not quantified; nd = not detected.
* Unaltered opaque phases. The unaltered Fe-Ni metal is only in the W2 part of the section; in the most weathered part of the section (W4) all the Fe-Ni metal is completely altered whereas little amounts of unaltered phosphides (and sometimes sulphides) may still survive.

Table 3 – Representative olivine compositions (wt%) from Acfer 370.

SiO_2	41,65	42,40	41,78	42,08	40,99	41,96	41,31	42,23	41,89	41,48	41,38	40,49	42,45	40,46	41,50	41,31
Cr_2O_3	–	0,07	–	0,07	–	–	0,07	–	–	–	–	0,07	–	–	–	–
FeO	5,37	5,23	5,16	5,79	5,53	5,75	5,64	5,36	5,47	5,87	5,62	5,63	5,78	5,52	5,43	5,47
MnO	0,48	0,44	0,44	0,43	0,44	0,41	0,39	0,46	0,47	0,50	0,50	0,48	0,49	0,44	0,43	0,47
MgO	53,05	52,77	52,29	52,52	51,21	53,04	52,23	53,01	51,64	54,36	52,08	52,02	53,44	51,43	51,61	52,11
Total	100,55	100,91	99,67	100,89	98,17	101,16	99,64	101,06	99,46	102,21	99,58	98,69	102,16	97,85	98,97	99,36
Fa*	5,4	5,2	5,2	5,8	5,7	5,7	5,7	5,3	5,6	5,7	5,7	5,7	5,3	5,6	5,5	5,5

Cr_2O_3 detection limit is 0.06 wt%. The following elements have not been reported since they were always below detection limits: Al_2O_3 (0.04), TiO_2 (0.05), CaO (0.04), CoO (0.08), NiO (0.10), V_2O_5 (0.12).
* mol%

Table 4 – Representative pyroxene compositions (in wt%) from Acfer 370. The simplified nomenclature from Morimoto et al. (1988) has been adopted.

	Enstatite													Pigeonite			Augite							
SiO_2	57,32	57,23	56,43	57,42	56,43	57,65	55,39	56,99	56,31	56,05	56,45	53,85	53,49	56,88	57,20	55,17	54,49	52,44	52,97	51,49	53,69	51,72	52,67	46,02
TiO_2	0,06	–	–	–	–	–	–	–	–	0,08	–	0,14	0,08	0,10	0,15	0,24	0,22	0,18	0,14	0,52	0,26	0,73	1,13	1,08
Al_2O_3	0,40	0,11	0,16	0,07	0,19	0,18	0,16	0,57	0,60	0,85	0,42	2,21	0,71	0,54	1,96	1,37	0,73	0,61	0,50	1,63	1,28	5,23	7,76	11,21
Cr_2O_3	0,36	0,25	0,59	0,30	0,36	0,22	0,33	0,68	0,65	0,60	0,61	1,32	0,53	0,54	1,00	1,63	2,42	1,42	1,52	1,05	2,20	2,58	0,37	0,77
FeO	6,24	9,49	10,74	10,76	7,03	7,31	13,62	11,04	10,34	10,07	12,36	11,94	20,31	8,70	6,56	5,80	9,70	14,40	12,77	8,97	8,63	3,08	0,77	7,20
MnO	0,55	0,47	0,30	0,59	0,72	0,65	0,81	0,28	0,27	0,30	0,53	0,27	0,33	0,67	0,83	0,85	0,57	1,03	0,76	0,91	0,61	0,80	0,13	0,20
MgO	33,61	32,89	30,67	32,04	33,17	32,73	27,74	31,45	30,09	30,77	29,74	26,92	21,47	31,33	28,41	25,44	20,76	15,35	15,56	16,63	15,70	18,56	18,13	12,65
CaO	0,19	0,22	0,23	0,24	0,30	0,33	0,51	0,66	0,70	0,98	1,05	1,64	1,78	2,86	3,96	7,70	11,94	13,77	15,67	15,33	17,41	17,39	19,25	19,11
Na_2O	–	–	–	–	0,20	–	–	–	–	–	0,17	–	–	0,16	–	0,65	0,98	0,85	0,71	0,75	1,02	0,87	1,04	–
Total	98,74	100,66	99,11	101,42	98,42	99,06	98,56	101,67	98,96	99,81	101,33	98,32	98,70	101,78	100,07	98,85	101,81	100,05	100,60	97,27	100,80	100,96	101,25	98,25
Wo*	0,37	0,41	0,45	0,45	0,58	0,64	1,03	1,24	1,38	1,90	2,02	3,39	3,75	5,37	8,15	16,17	24,67	29,70	33,14	33,71	37,86	38,12	42,70	45,14
En*	90,24	85,71	83,21	83,77	88,86	88,30	77,60	82,51	82,68	82,89	79,46	77,36	62,88	81,87	81,32	74,33	59,68	46,06	45,78	50,89	47,50	56,61	55,96	41,58
Fs*	9,40	13,87	16,35	15,78	10,56	11,06	21,37	16,25	15,94	15,22	18,53	19,25	33,37	12,75	10,53	9,51	15,64	24,24	21,08	15,40	14,65	5,27	1,33	13,28

Detection limits (wt%): TiO_2 (0.05); Na_2O (0.16). K_2O has been omitted because it was always below detection limit (0.08).
* Wo, En and Fs are expressed in mol%

Table 5 – Phosphides, metal and sulphides compositions (in wt%) from Acfer 370; the table also include some analyses of schreibersite in NWA 7135. No analyses of metal and troilite have been reported for NWA 7135 since the specimen observed is completely weathered (W4) and these minerals have been replaced by terrestrial products.

	Schreibersite			Schreibersite (NWA 7135)				Nickelphosphide				Fe-Ni metal									Troilite			
Si	0,05	0,05	0,05		_	_	_	0,05	–	–	–	0,05	–	–	–	–	–	–	–	–	–	–	–	–
P	14,25	14,94	14,91	17,33	16,84	16,59	16,63	14,37	13,78	14,47	14,40	0,15	–	–	0,11	–	0,05	0,09	0,11	0,13	–	–	–	–
S	–	0,08	0,05					0,05	0,06	0,04	0,07	0,04	–	–	–	–	0,04	–	–	–	36,03	36,64	36,15	36,84
Cr	_	_	_					_	_	_	_	_	_	_	_	_	_	_	_	_	0,27	0,32	0,30	0,33
Fe	41,44	44,09	44,91	46,35	46,53	46,62	47,77	38,11	41,18	40,32	40,44	93,94	94,09	93,07	93,37	93,88	93,63	92,94	93,05	93,58	63,54	62,16	62,65	62,26
Co	_	_	_					_	_	_	_	0,37	0,37	0,43	0,30	0,31	0,32	0,34	0,35	0,33	_	_	_	_
Ni	41,93	41,10	40,63	36,32	36,63	36,79	35,60	45,51	43,66	43,31	44,02	6,33	6,21	6,13	6,09	6,23	6,34	6,27	6,06	6,32	_	_	0,34	_
Total	97,67	100,26	100,55					98,09	98,70	98,15	98,95	100,88	100,68	99,64	99,87	100,43	100,39	99,65	99,57	100,35	99,79	99,04	99,35	99,48

Detection limits (wt%): Si (0.05); P (0.05); S (0.04); Cr (0.07); Co (0.10); Ni (0.12). The following elements have not been reported since they were always below detection limits: Mn (0.08), Cu (0.13), Zn (0.13).

Table 6 – Trace-elements concentration (μg/g)

	Acfer 370	[1]El Médano 301	[2]BIR-1 (SH)	[2]W2 (SH)	[2]DNC-1 (SH)	[2]BHVO-2 (SH)	[2]AGV-1 (SH)
Li	2.87	2.65	3.54	9.86	5.07	4.37	11.15
Be	–	0.04	–	–	–	–	–
Sc	6.96	5.5	43.9	9.86	31.5	30.1	12.8
Ti	530	–	6096	36.1	2979	16219	6738
V	63.8	41	322	6584	148	307	129
Cr	2753	–	392	265	281	281	8.61
Mn	2242	–	1331	91.0	1149	1270	791
Co	726	–	51.2	1301	56.4	43.0	15.4
Ni	14533	–	165	44.0	261	109	14.8
Cu	140	72	125	66.6	103	128	61.1
Zn	21.0	–	69.5	108	65.2	97.1	93.8
Ga	2.40	5.9	14.9	76.5	13.2	20.0	21.7
Rb	1.75	2.71	0.189	17.3	3.51	8.48	68.5
Sr	48.2	23.1	107	19.1	141	365	677
Y	2.13	2.04	16.8	190	19.0	26.6	21.6
Zr	5.55	5.9	15.7	23.2	36.5	163	242
Nb	0.43	0.37	0.688	87.9	1.60	18.6	15.8
Mo	1.46	4.1	0.102	7.66	0.140	3.92	2.43
Sn	4.10	–	1.42	0.462	1.99	1.88	4.57
Sb	0.158	–	0.368	2.65	0.809	0.053	4.41
Cs	0.076	0.516	0.004	0.573	0.207	0.086	1.28
Ba	408	105	5.81	0.867	93.4	113	1207
La	0.357	0.609	0.592	154	3.65	14.6	39.3
Ce	0.914	1.56	1.92	10.3	8.45	35.6	71.4
Pr	0.127	0.188	0.364	23.1	1.08	4.95	8.46
Nd	0.650	0.828	2.41	2.91	5.09	23.7	33.2
Sm	0.217	0.229	1.12	13.1	1.50	5.97	6.11
Eu	0.088	0.087	0.521	3.36	0.597	1.98	1.69
Gd	0.278	0.311	1.87	1.11	2.08	6.01	4.90
Tb	0.050	0.054	0.377	3.71	0.410	0.923	0.682
Dy	0.335	0.341	2.58	0.641	2.80	5.08	3.66
Ho	0.075	0.074	0.603	3.84	0.671	0.974	0.721
Er	0.221	0.222	1.74	0.825	1.99	2.46	1.90
Tm	–	0.033	–	–	–	–	–
Yb	0.210	0.208	1.6622	2.11	1.95	1.89	1.72
Lu	0.034	0.033	0.2592	0.310	0.311	0.272	0.256
Hf	0.164	0.170	0.6243	2.34	1.03	4.23	5.25
Ta	0.039	0.025	0.1011	0.554	0.111	1.15	0.936
W	–	0.27	–	–	–	–	–
Tl	0.022	–	0.0012	0.097	0.025	0.02	0.349
Pb	9.02	0.97	2.9668	7.16	5.97	1.68	37.2
Th	0.052	0.115	0.039	2.16	0.259	1.19	6.53
U	0.159	0.061	0.011	0.479	0.059	0.39	1.91

[1] Data from Pourkhorsandi et al. (2017)
[2] Calibration standards used for analyses

Table 7 - Oxygen isotope analyses for EATG-washed material from Acfer 370

SAMPLE	**$\delta^{17}O$‰**	1σ	$\delta^{18}O$‰	1σ	$\Delta^{17}O$‰	1σ
Acfer 370	3.068		4.460		0.749	
Acfer 370	2.827		4.110		0.690	
Acfer 370	2.738		4.108		0.602	
Mean values	**2.878**	**0.171**	**4.226**	**0.203**	**0.680**	**0.074**

Table 8 – Compositional range of the main and accessory phases in forsterite-rich ungrouped meteorites.

		Acfer 370	[1]Cumberland Falls inclusions	[1]ALHA 78113 inclusions	[2]NWA 7135	[3]El Médano 301
Olivine	(Fa)	5.2-5.8	1-5	2-21	4.8-6.2 (rarely >6.2)	3.5-5.0
Enstatite	(En) (Fs) (Wo)	62.9-90.2 9.4-33.4 0.4-3.7	 0.3-14.5 0.4-1.0	 3-26	 7-21.8 0.4-1.5	 7.4-18.8
Pigeonite	(En) (Fs) (Wo)	74.3-81.9 9.5-12.7 5.4-16.2			 17.3 6.9	
Sub-calcic augite	(En) (Fs) (Wo)	46.1-59.7 15.6-24.2 24.7-29.7			 13.3-22.2 25.4-29.9	
Augite	(En) (Fs) (Wo)	41.6-56.6 1.3-21.1 33.1-45.1	 0.22 40.1	58 40		
Diopside	(En) (Fs) (Wo)	41.4 13.6 44.9				
Jadeitic pyroxene	(Wo) (Fs) (Ja)		3.6-22.0 4.6-14.9 8.5-35.4			
Plagioclase and plagioclase-glass	(An)	8-34	4-11	0.6-23		
[4]Iron	(Ni) (Co) (Si)	6.1-6.3 0.30-0.43	4.4-5.8 0.38-0.53 0.08-0.24	3.4-6.3		5.7-6.7
[4]Troilite	(Ni) (Cr)	<0.12-0.34 0.27-0.33	<0.02	<0.02-0.58		
[4]Schreibersite / Nickelphosphide	(Ni)	40.6-45.5	30-53	0.0-33	35.6-36.8	
Phosphate		hydroxylapatite	0.0	brianite-merr		chlorapatite

Data from: [1]Lipschutz et al. (1988); [2]Irving et al. (2015); [3]Pourkhorsandi et al. (2017)
[4]The contents of Ni, Co, Cr, Si, have been expressed as wt%.

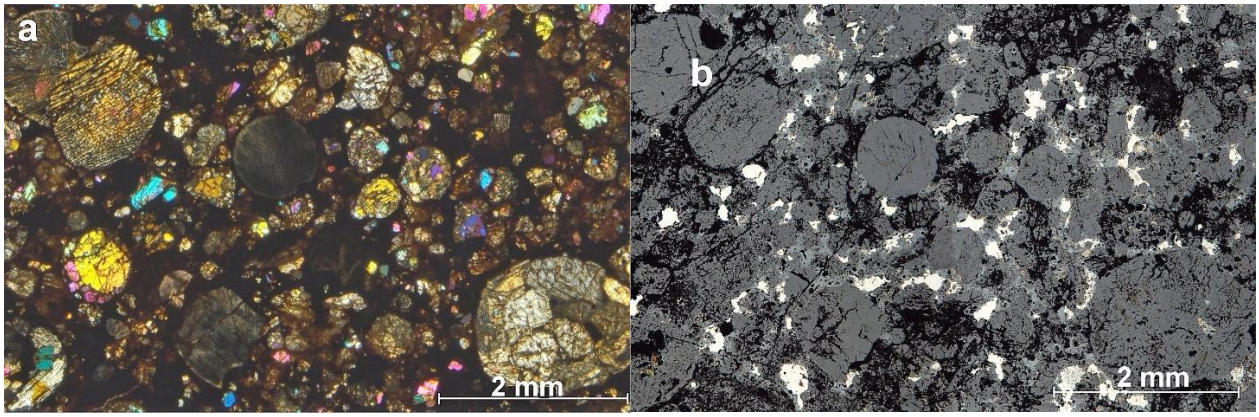

Figure 1 – Acfer 370: a) Transmitted cross-polarized light image of a small portion of Acfer 370 showing olivine- and pyroxene-bearing chondrules; b) the same area, as seen in plane polarized reflected light, displays silicates (dark gray), Fe-oxides (pale gray), metal and troilite grains (respectively white and white yellowish).

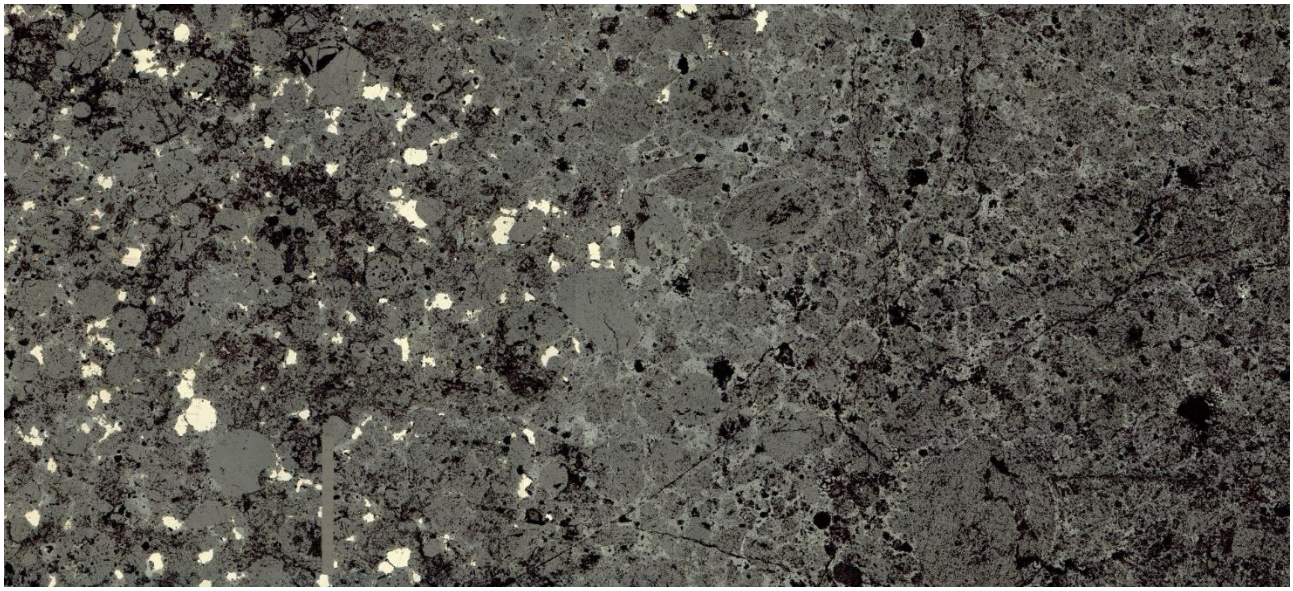

Figure 2 – Optical microscopy (reflected light) photomosaic image of a thin section of Acfer 370. Two areas, with different weathering grades, can be easily seen: in the left part of the image, where a lesser amount of weathering is present, metal and sulfide (bright white spots) still survive and the grade is W2; in the central and right part, the opaque phases have been completely oxidized and transformed into Fe-oxyhydroxides yielding a W4 grade. The occurrence of such sharp contact is due to a main fracture along with a fracture system (probably a thermal cracking) that affected the two portions of the meteorite differently. Despite this sharp difference, both the areas have been carefully studied and no discontinuities, neither in mineralogy nor in petrology, have been detected. Field width 17 mm.

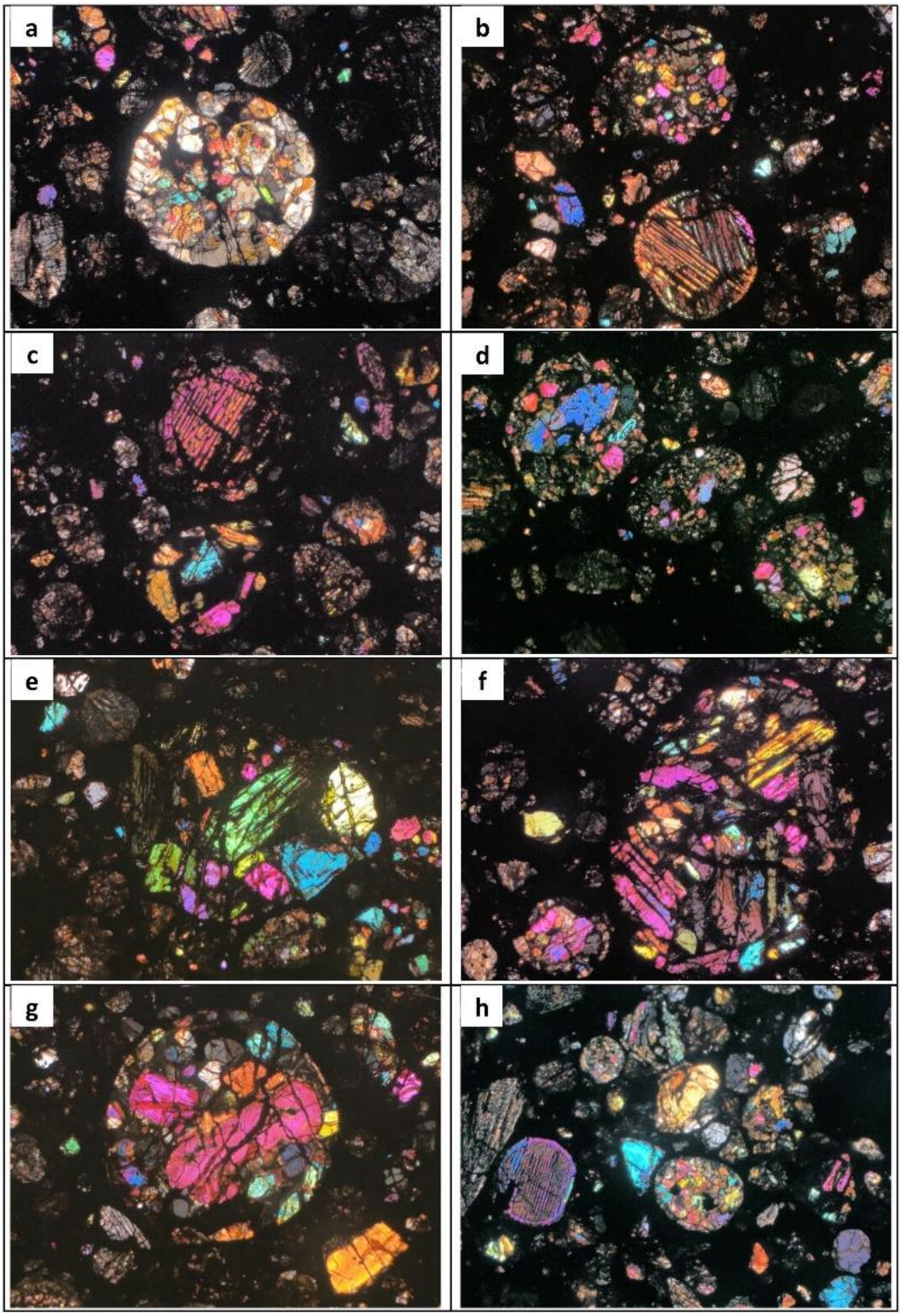

Figure 3 – Chondrule types observed in Acfer 370 (transmitted light, crossed polars; 50X): a) poikilitic pyroxene; b) POP and BO; c) PO and BO; d) POP, GO, GOP; e,f,g) PO; h) BO and GOP.

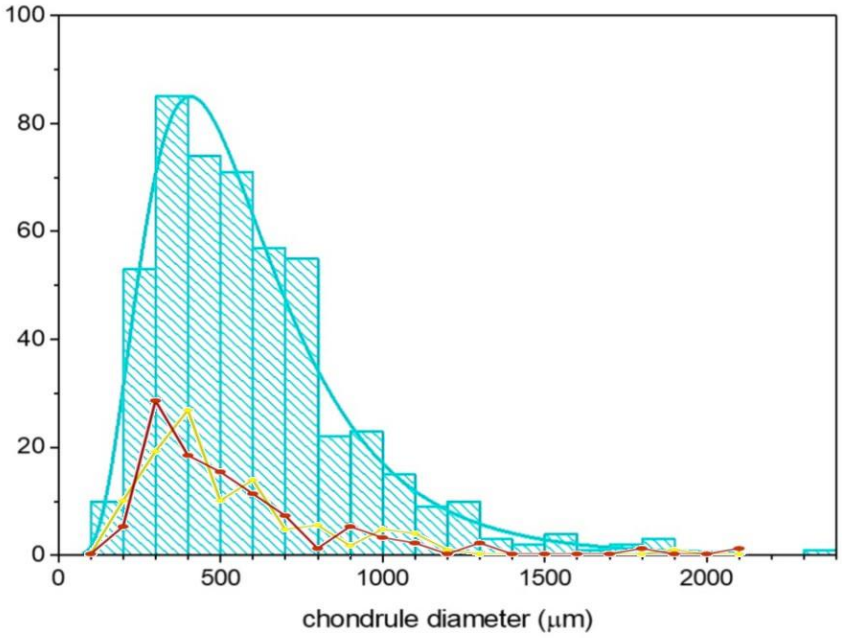

Figure 4 – Distribution of all occurring types of chondrules in Acfer 370 (light blue), NWA 7135 (yellow), El Médano 301 (red). Data of size distribution in El Médano 301 and NWA 7135 are from Pourkhorsandi et al. (2017).

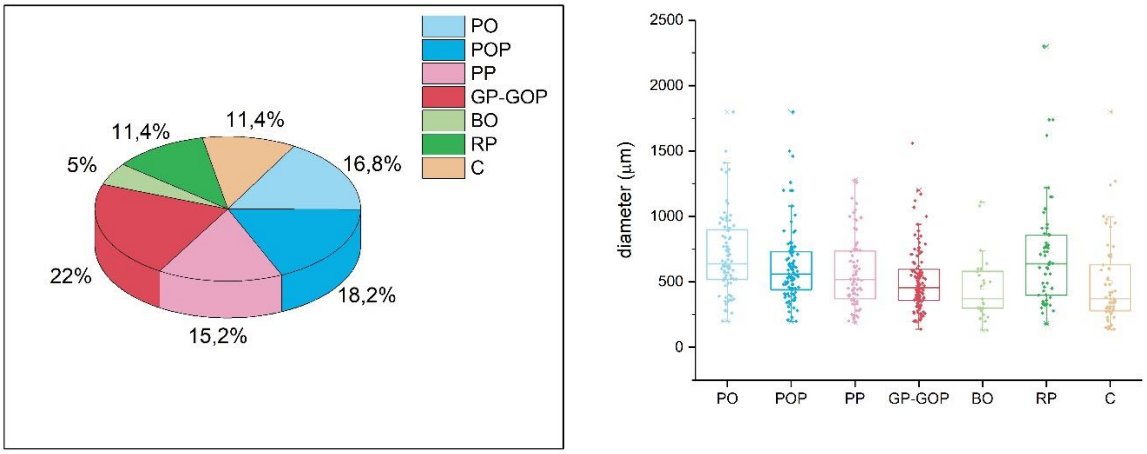

Figure 5 – Abundance of different types of chondrules (left) and relative size distribution (right) in Acfer 370. The diagrams display the results of the study performed on 500 chondrules.

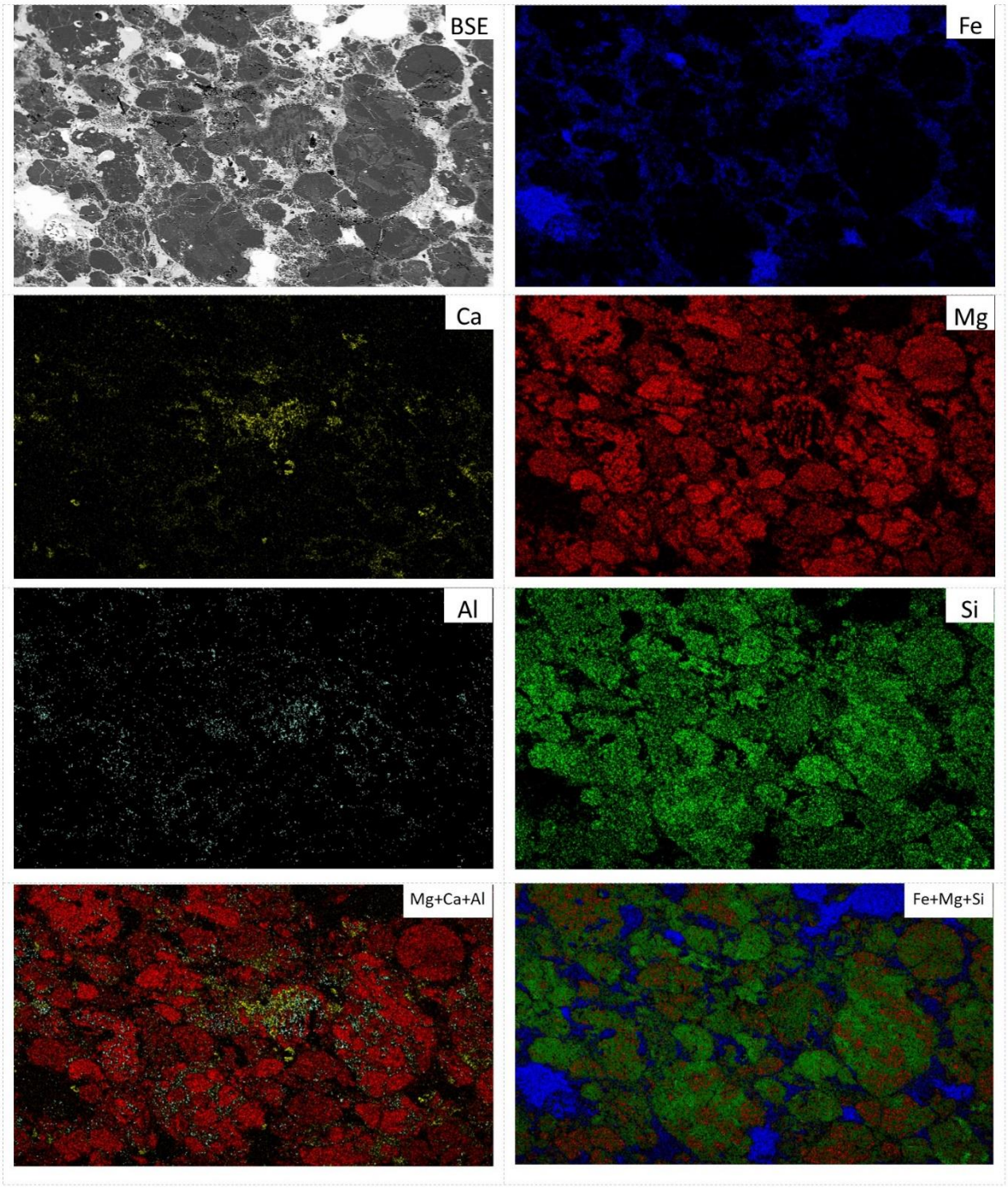

Figure 6 – Backscattered electron image and X-ray elemental maps of Acfer 370 (field of view 3 x 1.8 mm). Distribution of major phases (low-Ca pyroxenes, Fe metal, olivine, plagioclase and feldspathic glass, high-Ca pyroxenes) can be inferred from the map. The bottom figures are RGB maps obtained by the overlay of X-ray elemental maps showing the abundance of the main silicate phases and metal: in particular, in the bottom-left figure mesostasis (mostly devitrified feldspar normative glass containing high-Ca pyroxenes and albitic plagioclase microlites), can be seen represented in cyan, and the high-Ca pyroxene in yellow; the bottom-right figure shows the distribution of low-Ca pyroxenes (green), olivine (brown) and metal (blue).

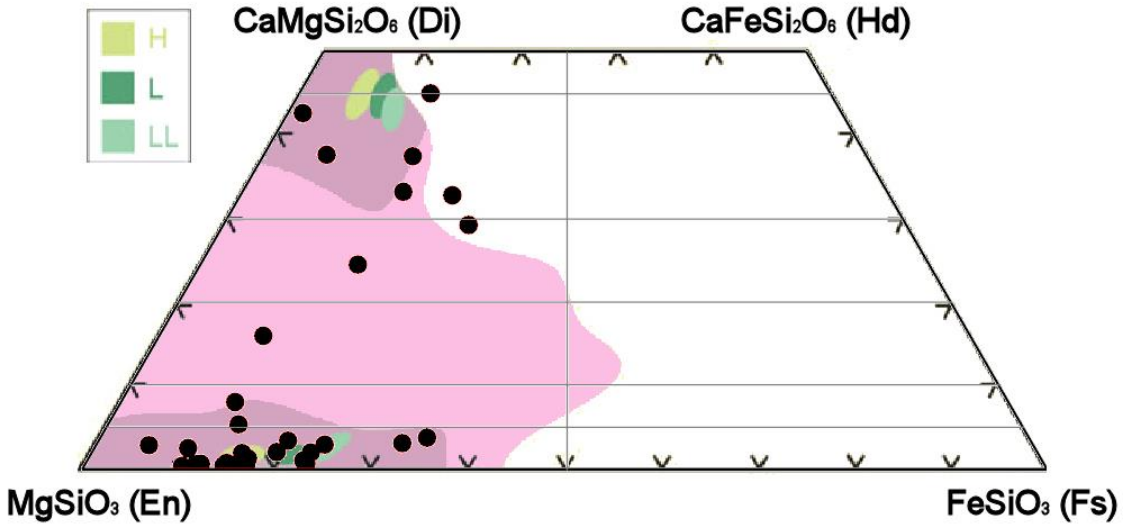

Figure 7 – Pyroxenes quaternary diagram representing the compositional fields adopted by Rock (1990). The compositions of Acfer 370 (black dots) have been superimposed to the composition of pyroxenes in unequilibrated (UOC) and equilibrated (EOC) ordinary chondrites. The pale pink color field, that covers most of the low-iron part of the quadrilateral, is the area throughout which very few compositions of pyroxenes in UOC fall; the vivid pink parts of the field are where most of the data plot (modified from Grady et al. 2014). The shaded areas are representative of the pyroxenes compositions of enstatite chondrites.

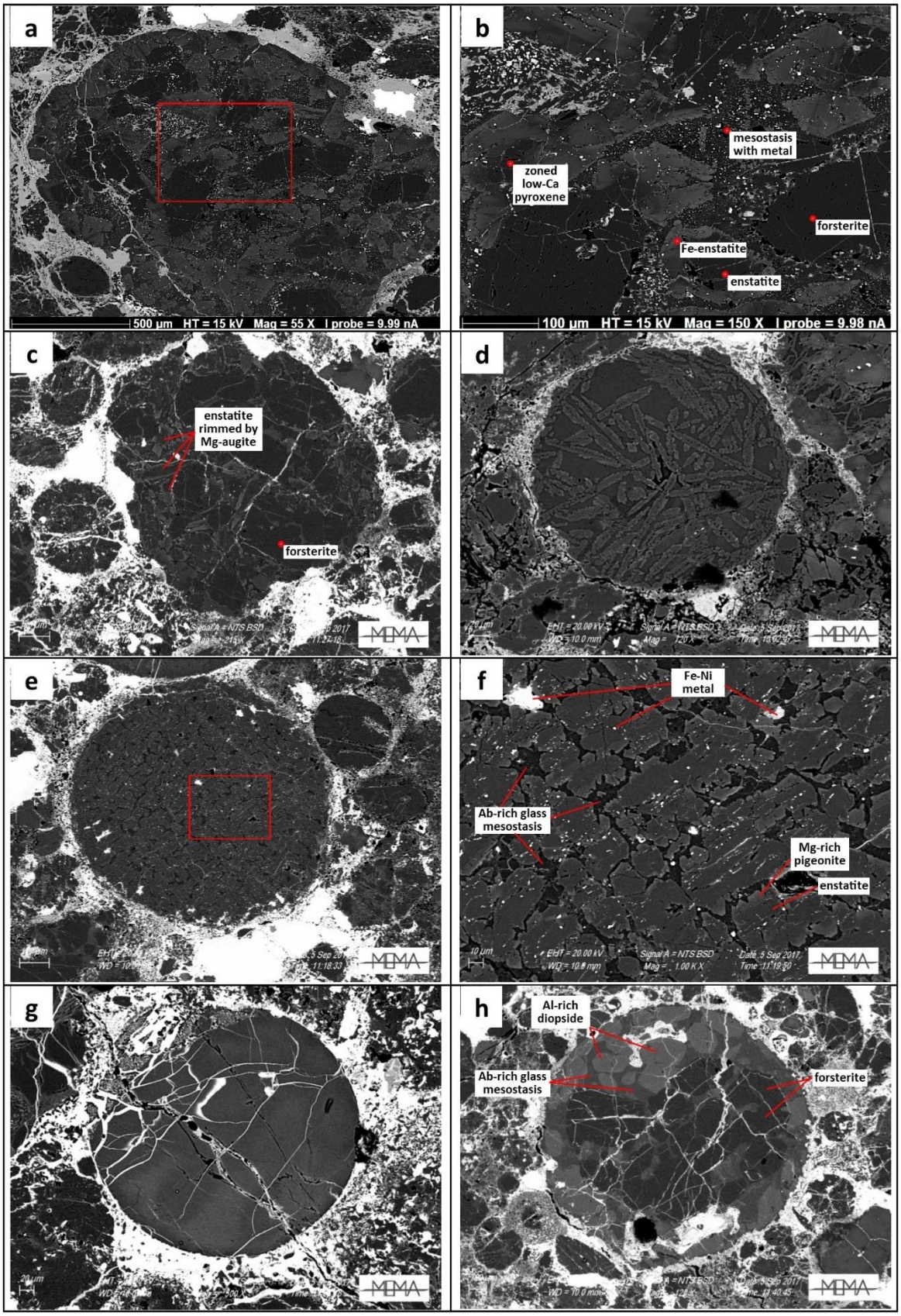
a
500 µm HT = 15 kV Mag = 55 X I probe = 9.99 nA
b
mesostasis with metal
zoned low-Ca pyroxene
forsterite
Fe-enstatite
enstatite
100 µm HT = 15 kV Mag = 150 X I probe = 9.98 nA
c
enstatite rimmed by Mg-augite
forsterite
d
e
f
Fe-Ni metal
Ab-rich glass mesostasis
Mg-rich pigeonite
enstatite
g
h
Al-rich diopside
Ab-rich glass mesostasis
forsterite

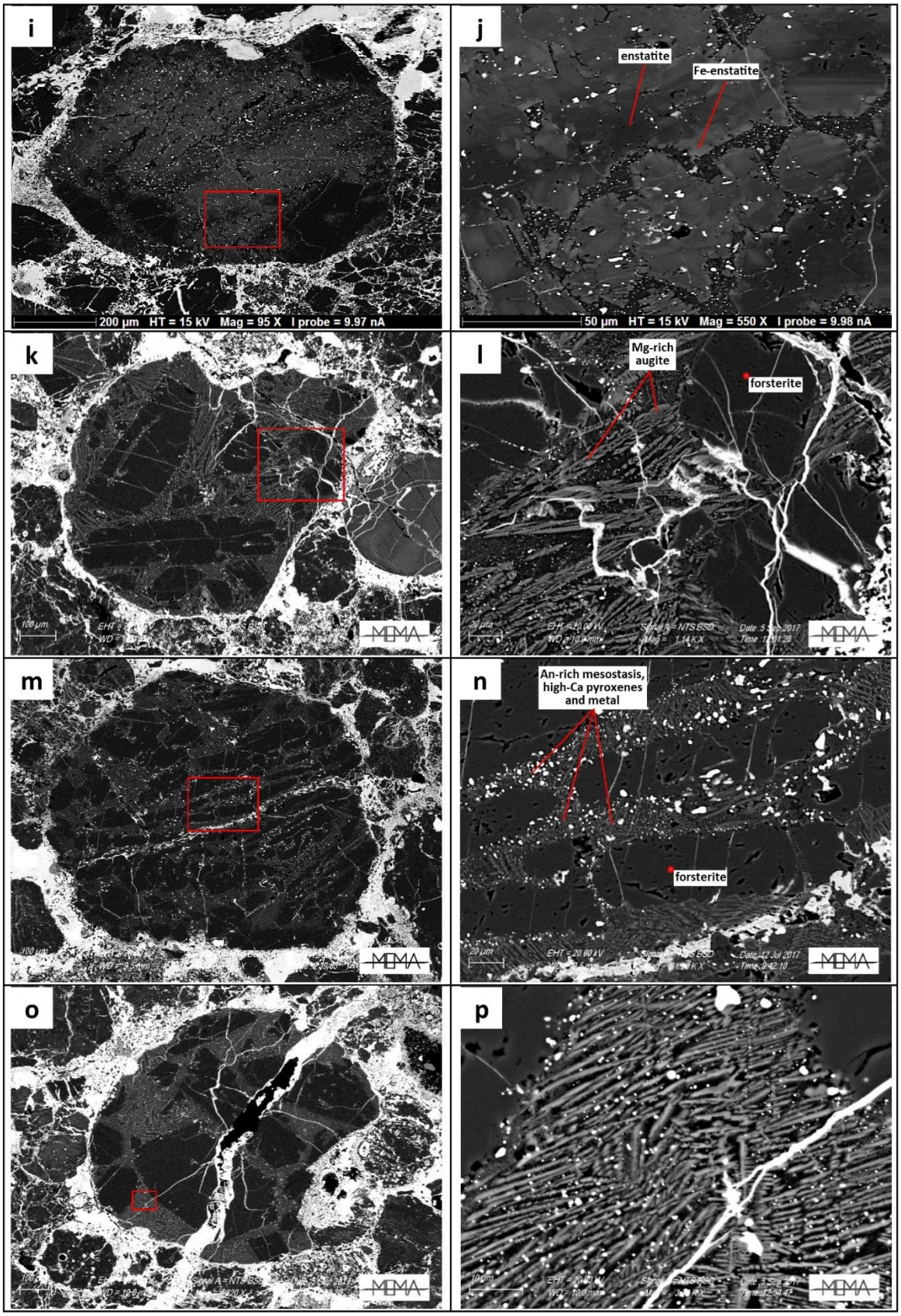
i
200 µm HT = 15 kV Mag = 95 X I probe = 9.97 nA
j
enstatite
Fe-enstatite
50 µm HT = 15 kV Mag = 550 X I probe = 9.98 nA
k
l
Mg-rich augite
forsterite
m
n
An-rich mesostasis, high-Ca pyroxenes and metal
forsterite
o
p

Figure 8 – Electron backscattered images of chondrules in Acfer 370. a) Chondrule with olivine (black) and pyroxene (gray) crystals: the particular (b) shows that euhedral olivine crystals and zoned low Ca-pyroxene (enstatite in the inner part and ferroan enstatite in the outer ones) are surrounded by interstitial mesostasis containing the most of metal; c) forsterite (dark gray) chondrule fragment along with enstatite rimmed by Mg-rich augite; d) elongated pyroxene calcian Mg-rich pigeonite laths (crystals) in a Na-Al rich (Ab_{79}) glass mesostasis; f) particular of the pyroxene chondrule (e) showing a normal zoning in pyroxene crystals: enstatite (dark gray) with external rim of Mg-rich pigeonite (light gray) and Na-Al rich (Ab_{92}) interstitial mesostasis (black); g) cryptocrystalline chondrule containing Na-Al (Ab_{66}) glass; h) euhedral and sub-euhedral crystals of forsterite (dark gray) and Al-diopside (light gray) in a plagioclase glass containing little grains of high-Ca pyroxenes; i) olivine-pyroxene chondrule characterized by large homogeneous forsterite crystals (black) and low-Ca pyroxene zoned crystals (gray): in the particular (j) the inner enstatitic portion and an outer ferroan enstatitic portion are well visible as well as the Na-rich glass; (k) chondrule characterized by large forsterite: in the particular (l) are visible skeletal Mg-rich augite crystals other than veins and little grains of metal; n) particular of the olivine chondrule (m) showing forsterite crystals (black) with interstitial Ca-Al glass mesostasis containing high-Ca pyroxene crystals and Fe-Ni metal grains; o) chondrule with large forsterite crystals (black): the particular (p) put in evidence the Ca-Al glass containing skeletal crystals of diopside.

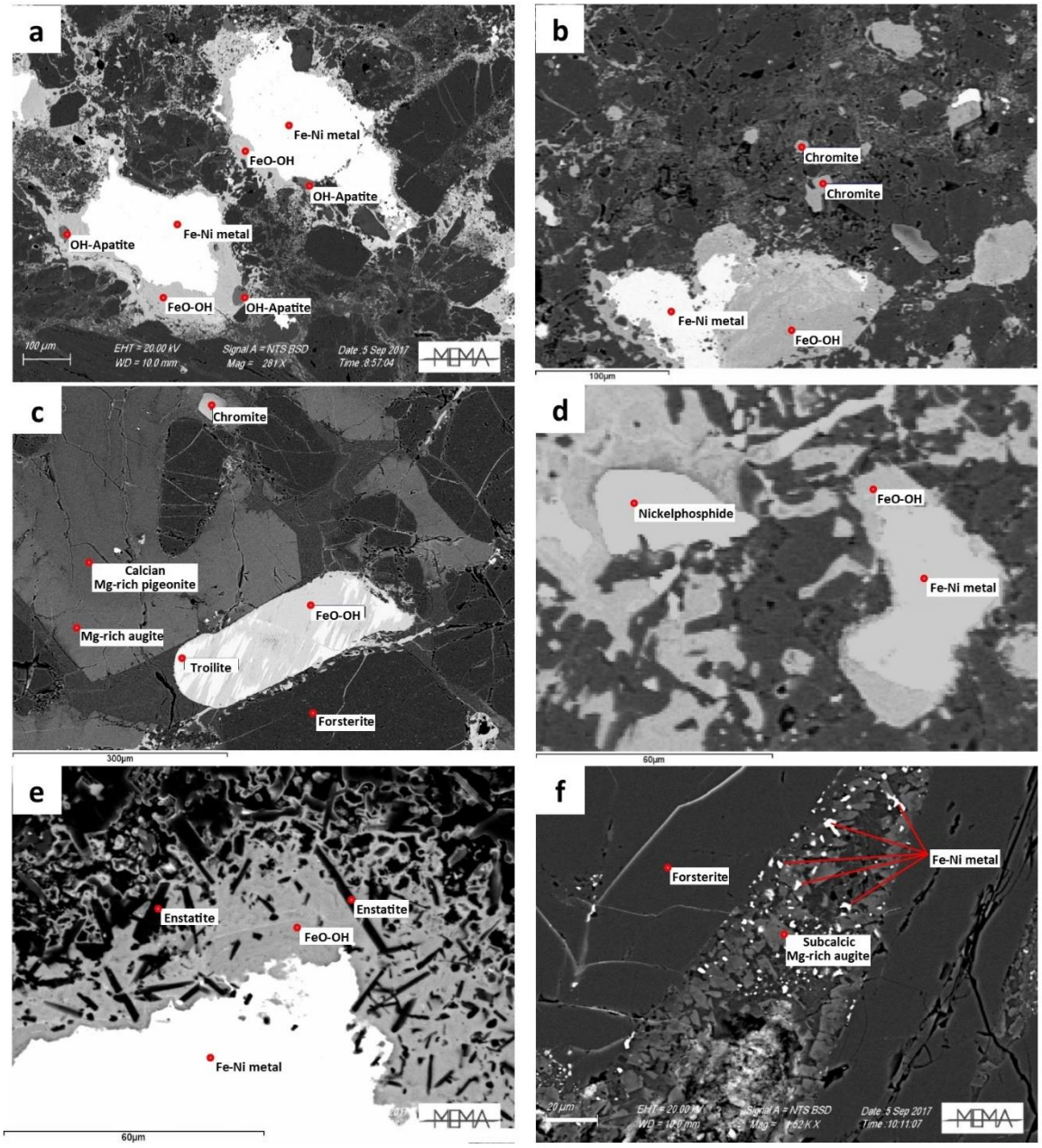
a
Fe-Ni metal
FeO-OH
OH-Apatite
Fe-Ni metal
OH-Apatite
FeO-OH
OH-Apatite
100 µm
EHT = 20.00 kV
WD = 10.0 mm
Signal A = NTS BSD
Mag = 281 X
Date :5 Sep 2017
Time :8:57:04
b
Chromite
Chromite
Fe-Ni metal
FeO-OH
100µm
c
Chromite
Calcian
Mg-rich pigeonite
FeO-OH
Mg-rich augite
Troilite
Forsterite
300µm
d
Nickelphosphide
FeO-OH
Fe-Ni metal
60µm
e
Enstatite
Enstatite
FeO-OH
Fe-Ni metal
60µm
f
Forsterite
Fe-Ni metal
Subcalcic
Mg-rich augite
20 µm
EHT = 20.00 kV
WD = 10.0 mm
Signal A = NTS BSD
Mag = 1.62 K X
Date :5 Sep 2017
Time :10:11:07
g
Oldhamite
h
i

Figure 9 – a) Hydroxylapatite grains distributed on the margin of Fe-Ni metal (most of them inside the iron oxide-hydroxide weathering products); b) euhedral and sub-euhedral chromite crystals; c) elongated troilite grain strongly affected by weathering; d) nickelphosphide grain showing a rim of alteration; e) lath-shaped crystals of enstatite inside iron oxide-hydroxide (silicate-metal intergrowth similar to that observed in some enstatite chondrites); f) blebs of Fe-Ni metal inside and outside subcalcic Mg-rich augite (scale bar on the left is 20 μm); g) oldhamite grains (the largest one is about 200 μm) along with X-ray maps of Ca (h) and S (i).

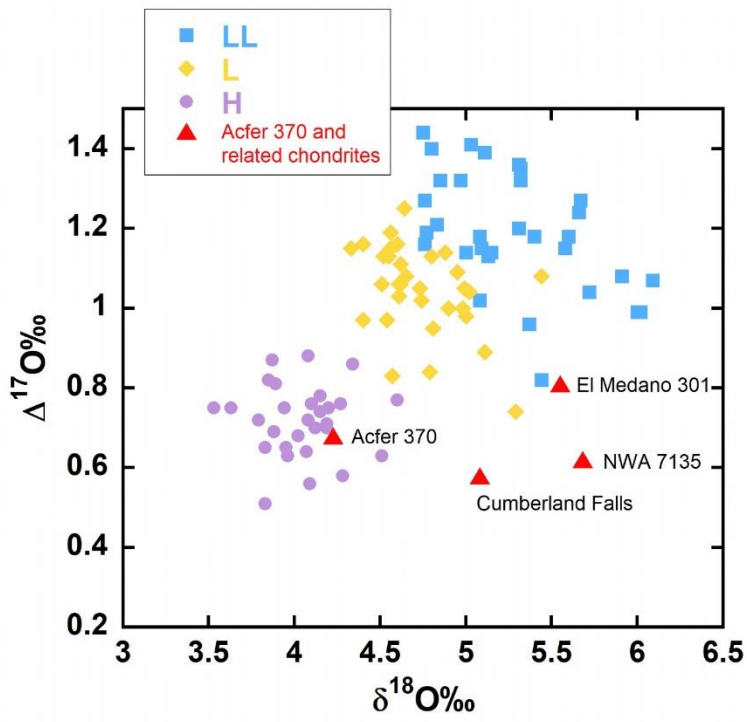

Figure 10 – Oxygen isotope composition of Acfer 370 and related ungrouped chondrites shown in relation to the H, L and LL group chondrite analyses of Clayton et al. (1991). Data sources: Cumberland Falls chondritic inclusions: Kuehner et al. (2016); NWA 7135: Irving et al. (2015), Kuehner et al. (2015); El Medano 301:Pourkhorsandi et al. (2017).